FLOW IN VENTILATING DUCTS

FLOW IN VENTILATING DUCTS
OF ELECTRICAL MACHINERY

By

LESLIE C. GALLOWAY, B.A.Sc.

A Thesis

Submitted to the Faculty of Graduate Studies

in Partial Fulfilment of the Requirements

For The Degree

Master of Engineering

McMaster University

May, 1969

MASTER OF ENGINEERING (1969) McMASTER UNIVERSITY
Hamilton, Ontario

TITLE: FLOW IN VENTILATING DUCTS OF ELECTRICAL MACHINERY

AUTHOR: Leslie C. Galloway, B.A.Sc. (University of British Columbia)

SUPERVISOR: Assistant Professor, Dr. B. Latto

NUMBER OF PAGES: vii, 60

SYNOPSIS:

This thesis describes an experimental study of the air flow in the ventilating ducts in the stators of electric motors and/or generators of a conventional design. The objective was to facilitate prediction of local heat transfer coefficients in ventilating ducts. Various flow phenomena were observed and compared with theoretical predictions. While the theory usually used for similar cases was found to be inapplicable, a related theory was found that checked well with experimental results. A stall phenomenon was observed under certain identified conditions. Useful relationships for predicting the flow details were obtained. The relevance of the work is discussed and future work is proposed.

ACKNOWLEDGEMENTS

The author is indebted to Dr. B. Latto who, as supervisor, provided invaluable guidance in the experimenting, in the analysis, and in the rendering of the results into intelligible form.

Canadian Westinghouse Company Limited, The Ford Foundation, and the Department of University Affairs of Ontario provided financial assistance for this project.

TABLE OF CONTENTS

NOTATIONS

a	duct width
b	air gap channel width
C_m	coefficient of mixing zone width
C_c	coefficient of contraction
$F[\ ]$ or $F_x[\ ]$	a function, defined when introduced where necessary, x takes different meanings
f, g	ordinates of sources and sink in the ξ plane
e	general expression for f, g, etc.
h	static head, sometimes subscripted - inches of water
$H_e[\ ]$	a function defined in (16)
m	source strength
p	static pressure, sometimes subscripted to identify location or state
Q	rate of volume flow, sometimes subscripted
r	ratio of density to density at N.T.P. (.075 lb_m/ft^3)
s	distance along mixing zone
t	transformation parameter
u	complex velocity
v_x, v_y	x, y direction components of velocity
v	velocity, sometimes subscripted to identify location
w	complex potential
x, y	coordinates of a point
z	complex location of a point
γ	ratio of pressure drop to dynamic head in jet

ζ	transformation parameter
η	dimensionless distance across jet
ξ	dimensionless distance across mixing zone
ρ	density
ϕ	potential function
χ	coefficient of flow in mixing zone
ψ	stream function
Ψ	dimensionless pressure integral from (20)

Subscripts

1	upstream end of air gap	- B in Figure 5
2	downstream end of air gap	- C in Figure 5
j	at vena contracta	- EF in Figure 5
d	downstream end of vent-duct	

ILLUSTRATIONS

FLOW IN VENTILATING DUCTS OF ELECTRIC MACHINERY

by L. C. Galloway

GENERAL APPROACH AND PRELIMINARY OBSERVATIONS

Introduction

With a high-speed computer the temperature distribution in the armature of an electric motor or generator can be calculated if values of heat generation, thermal conductivity and heat transfer coefficients are known. Unfortunately, these parameters and, in particular, the coefficients of heat transfer from the stator surfaces to the ventilating air, are not well-known.

It is reasonable to precede the study of the heat transfer coefficients with a detailed investigation of the flow of the ventilating air. Such an investigation is the subject of this thesis. Its objective was to discover the details of flow in the conventional radial stator ventilating ducts.

The strategy of the investigation involved four steps. The first step was to build a model of a ventilating duct simulating, as nearly as feasible, the conditions in a prototype motor. The second was to observe the flow occurring in the model. The third was to develop a mathematical theory of the flow observed. Finally, quantitative measurements were to be obtained to test the theory.

The flow patterns discovered were surprisingly complex and will significantly affect heat-transfer phenomena. The theories usually used for this type of flow (free stream theories) were found to be inapplicable. However a theory of apparently general application was found which checks well with the observations.

Model Description

Figures 1 and 2 show the model that was used which was an accurate reproduction of a typical ventilating duct used in a 5000 hp motor. The duct was the portion ABCD between two spacers (or 'vent fingers') and was divided at the air gap end into two smaller ducts by the block which simulated the armature coil. A blower drew the air through the ventilating duct at various velocities typical of those used in practice.

In an actual motor a vent duct is only one of a cascade of such ducts around the periphery of the stator. Partial ducts, called guards, situated on each side of the duct which was tested, simulated this condition. Air was drawn through these by a separate blower.

A channel crossing the inlet end of the ventilating duct simulated the air-gap. Air was drawn through it by another blower at various velocities which were typical of about half the peripheral speed of an actual rotor.

Figure 3 shows the model, test rig and instruments.

Visual Tests

Various methods of flow visualization were tried.

Smoke proved to be useless at the air velocities used in the model because it was dissipated too rapidly. A short tuft of thread attached to the end of a thin wand was useful for roughly determining local flow directions and disturbances. The most useful method was to inject particles of farina into a region known to be quiescent and to observe the paths of these particles.

Ideally the particles used for flow visualization should have a density approximately that of air but this was not feasible to achieve. Farina was the most useful and convenient material tested since it is reasonably free of dust, consistent in size and has little tendency to stick to surfaces. Its terminal velocity is about 3 feet per second, or about one-tenth of the lowest air velocity being observed, and therefore it followed the air streams closely enough to show the main features of the flow patterns.

Visual Observations

With some variation the flow pattern had similar features for all test conditions except when the duct was stalled or when no flow was induced in the air gap.

When external means were not used to induce flow in the air gap, air entered the vent duct as it would into a sharp-edged orifice separating from the four corners of the entrance and flowing with a symetrical velocity distribution. However, when flow was induced in the air gap the pattern changed drastically to that shown in figure 4. In each duct flow separated at corner A and entered the duct with a high velocity jet that contracted to a vena contracta at E.

Examination of tuft behaviour revealed that a separation occurred from the left wall just downstream of the vena contracta. At that point the jet separated from the wall to cross the duct and reattached to the wall at F about 1 1/2 to 2 duct widths from the entrance. Usually the jet was not dissipated when it had reached the point of reattachment and it started back across the duct. There was a spiral motion in the flow downstream from the reattachment.

Between the corner of separation and the point of reattachment, was a relatively quiescent zone which was bounded by the jet.

Stalling Condition

When the mean duct velocity was very low and/or the air gap velocity was very high the flow in the duct on one side of the armature coil stalled. This always occurred in the left duct of the model. All the flow passed on the other side of the armature coil. This stall would probably impair the cooling of the stator and the flow rate at which it occurs might occasionally be used in actual machines.

MATHEMATICAL ANALYSIS

Existing Mathematical Theories

The extensive literature on discontinuous flow and free-streamline solutions contains mathematical theories for the observed flow pattern. In particular the theories developed by McNown(1) and his associates(2)(3) at the Iowa Institute of Hydraulic Research are attractive. These described flow in a channel with a lateral connection closely corresponding to the air gap and ventilating duct. In their theories a free streamline was postulated and defined to be a streamline dividing a high velocity potential flow region (the jet) from a quiescent wake. The static pressure was postulated as continuous across and uniform along the streamline. The velocity in the jet was therefore required to be constant along the free streamline, from the point of separation to the vena contracta. The momentum change in the system was then equated to the integral of pressure about the system. The pressure integral was evaluated using a series of conformal transformations and, ultimately, parametric equations were found relating the dimensions of the channels, the various velocities, and the contraction coefficients.

Unfortunately, measured values from tests on the vent-duct model did not even approximately agree with the predictions of these equations. Further tests on the vent duct model revealed the reason. In the vent-duct model a free streamline, in the sense defined above, did not occur. Instead the high velocity jet was separated from the quiescent zone by a mixing zone across which the velocity change occurred. The width of this zone increased from zero at the entrance to about 30% of the duct width at the vena contracta. At the entrance the static pressure changed negligibly across the mixing zone. However, toward the vena contracta the mixing zone sustained a large pressure difference between the jet and the quiescent region. Accordingly, the pressure and the velocity were not uniform in the jet along the boundary streamline as was postulated in the free-streamline models.

Proposed Theory for Vent Ducts

Instead of using the free-streamline theory one can postulate a theory in which the velocity along the bounding streamline is allowed to vary. The theory can then be developed in a manner similar to that used by McNown and his associates but some empirical data might be required to complete the solution.

Consider the flow pattern shown in Figure 5 with the following assumptions:

(1) Fluid enters the channel across a plane B with a uniform velocity, v_1, and uniform pressure across this plane. Part of the fluid leaves crossing plane C with a uniform velocity, v_2, and the remainder leaves across plane EF across the jet with a uniform velocity, v_j.

(2) The fluid is incompressible and the flow is steady and body forces are negligible.

(3) In the region bounded by ABCDEFA flow is irrotational and viscous losses are negligible.

(4) At location A the static pressure is constant across the mixing zone AFG at some value, p_s. Elsewhere the mixing zone can sustain a difference of pressure.

Use the following definitions for a general point for which x and y are the coordinates of the point and v_x and v_y are the x and y components of velocity.

Location z is defined by

$$z = x + iy \tag{1}$$

Complex velocity u is defined by

$$u = v_x - i\, v_y \tag{2}$$

The potential function ϕ is defined by

$$v_x = \frac{\partial \phi}{\partial x} \qquad v_y = \frac{\partial \phi}{\partial y} \tag{3}$$

The stream function ψ is defined by

$$v_x = \frac{\partial \psi}{\partial y} \qquad v_y = -\frac{\partial \psi}{\partial x} \tag{4}$$

Finally, the complex potential w is defined by

$$w = \phi + i\psi \tag{5}$$

Now it can be shown that, for irrotational flow if the above definitions are used, (e.g. Robertson (4) page 85)

$$\frac{dw}{dz} = u \tag{6}$$

Bernoulli's Theorem, with the assumptions of negligible losses, and uniformity of velocity and pressure at plane B, gives for a general point in the region ABCDEFA,

$$\rho \frac{v^2}{2} + p = \rho \frac{v_j^{\,2}}{2} + p_j \tag{7}$$

where v_j and p_j are the velocity and pressure at the jet, plane EF. In particular at A there is a velocity, v_a, in the y direction and, since the pressure at A is p_s by postulate, then

$$\rho \frac{v_a^{\,2}}{2} + p_s = \rho \frac{v_j^{\,2}}{2} + p_j \tag{8}$$

From the condition of continuity and assumption of negligible density change

$$v_1 b = v_2 b + v_j\, C_c a \tag{9}$$

The momentum integral theorem states that, for the assumed conditions, the force equal to the summation of pressures and stresses integrated over the boundary equals the net rate of momentum convection out of the boundary. In particular, in the x direction

$$v_j^2 \rho C_c a = \int_{ABCDEFA} p\, dy \tag{10}$$

where C_c is the contraction coefficient defined by

$$Q_j = v_j C_c a \tag{11}$$

where Q_j is the flow rate from the jet.

The integral in equation (10) can be evaluated in three parts,

$$\int_{ABCDEFA} p\, dy = \int_{A..D} p\, dy + \int_{D..F} p\, dy + \int_{F..A} p\, dy \tag{12}$$

First consider the integral $\int_{A..D} p\, dy$

Using (7) and noting that

$$\begin{aligned} v^2 &= v_x^2 + v_y^2 \\ &= (v_x - iv_y)(v_x + iv_y) \\ &= u\,(v_x + iv_y) && \text{from (2)} \\ &= u\,(\tfrac{\partial\phi}{\partial x} + i\,\tfrac{\partial\phi}{\partial y}) && \text{from (3)} \end{aligned}$$

and that along boundary A..D

$$\int \frac{\partial\phi}{\partial x} dy = 0, \qquad \int u \frac{\partial\phi}{\partial y}\, dy = \int u\, d\phi$$

leads to

$$\int_{A..D} p\, dy = (p_j + \frac{\rho}{2} v_j^2)a - i\,\frac{\rho}{2} \int_{A..D} u\, d\phi \tag{13}$$

To evaluate $\int_{A..D} u \, d\phi$ the relationship between u and ϕ is required. This can be found by two conformal transformations.

$$t = (u/v_j)^2 \tag{14}$$

and

$$\zeta = 1/2 \left(t + \frac{1}{t} \right) \tag{15}$$

For convenience the values of the u, t and ζ at various points are depicted graphically in Figure 6. D' is the stagnation point that ends the streamline dividing the flow to the lateral from that continuing down the channel and is close to but not generally coincident with D. For convenience the values of these points in terms of the several parameters are tabulated in Table 1.

TABLE 1

Variable	A	B	C	D'	E or F
u	$-iv_a$	$-iv_1$	$-iv_2$	0	v_j
t	$-(v_a/v_j)^2$	$-(v_1/v_j)^2$	$-(v_2/v_j)^2$	0	+1
ζ	$-\frac{1}{2}\{(\frac{v_a}{v_j})^2 + (\frac{v_j}{v_a})^2\}$	$-\frac{1}{2}\{(\frac{v_1}{v_j})^2 + (\frac{v_j}{v_1})^2\}$	$-\frac{1}{2}\{(\frac{v_2}{v_j})^2 + (\frac{v_j}{v_2})^2\}$	$\pm\infty$	+1
		= f	= g		

These transformations are conformal and therefore sinks and sources in the physical plane are conserved in kind and magnitude in the transformations to the ζ plane. In the ζ plane solutions are readily found by superposition of known solutions. In particular the complex potential in the half plane of ζ caused by a source of strength m at location ζ_0 on the real axis is

$$w = \frac{m}{\pi} \text{Ln} [\zeta - \zeta_0]$$

Therefore by superposing similar expressions for a source of strength bv_1 at B, a sink of strength bv_2 at C and a sink of strength $C_c a v_j$ at E, in the ζ plane, an expression for w is found

$$w = \frac{1}{\pi} (b\, v_1 \text{ Ln} [\zeta - f] - C_c a\, v_j \text{ Ln} [\zeta - 1] - b\, v_2 \text{ Ln} [\zeta - g]) \qquad (16)$$

Along the boundary A..D in the ζ plane the stream function ψ is constant. Therefore

$$d\psi = 0$$

and

$$dw = d\phi + i\, d\psi = d\phi$$

whence, differentiating equation (16) gives

$$d\phi = dw = \frac{1}{\pi} \left(\frac{bv_1}{\zeta - f} - \frac{C_c\, a\, v_j}{\zeta - 1} - \frac{bv_2}{\zeta - g} \right) d\zeta$$

But $\qquad \zeta = \frac{1}{2} \{(u/v_j)^2 + (v_j/u)^2 \}$

and so

$$d\zeta = \left(\frac{u}{v_j^2} - \frac{v_j^2}{u^3} \right) du \qquad (17)$$

whence,

$$u\, d\phi = \frac{2}{\pi} (bv_1\, H_f[u] - C_c a\, H_1[u] - bv_2\, H_g[u])\, du \qquad (18)$$

where

$$H_e[u] = \frac{\left(\frac{u}{v_j}\right)^2 - \left(\frac{v_j}{u}\right)^2}{\left(\frac{u}{v_j}\right)^2 - 2e + \left(\frac{v_j}{u}\right)^2} \qquad (19)$$

Then, an approximate equation for the integral is

$$\int_{A..D} p\, dy = a \left(p_j + \rho \frac{v_j^2}{2}\right) - \rho \frac{i}{\pi} \left(bv_1 \int_{-iv_a}^{o} H_f[u]\, du - C_c a\, v_j \int_{-iv_a}^{o} H_1[u]\, du - bv_2 \int_{-iv_a}^{o} H_g[u]\, du\right) \qquad (20)$$

The approximation consists in using zero for the velocity at D, the upper limit of integration.

The integration and substitution of the limits are given in appendices 1 and 2 and are somewhat laborious, but when completed they give

$$
\begin{aligned}
\int_{A..D} p\,dy \;=\; & a\left(p_j + \rho\frac{v_j^2}{2}\right) \\
& - \frac{\rho}{\pi}\{\, b\,(v_1 v_a + v_1^2\,\mathrm{Tanh}^{-1}[v_1/v_a] + v_j^2\,\mathrm{Tanh}^{-1}[(v_a v_1)/v_j^2]) \\
& - C_c a\,(v_a v_j + 2v_j^2\,\mathrm{Tan}^{-1}[v_a/v_j]) \qquad (21) \\
& - b\,(v_2 v_a + v_2^2\,\mathrm{Tanh}^{-1}[v_1/v_a] + v_j^2\,\mathrm{Tanh}^{-1}[(v_a v_2)/v_j^2])\}
\end{aligned}
$$

The second component from equation (12) is simply

$$\int_{D..F} p\,dy = -p_j a C_c \qquad (22)$$

since v_j was assumed constant and this implies that p_j is constant across EF.

The solution of the third component, $\int_{F..A} p\,dy$, is more difficult since it is not know how p varies with y along AF and so it must be evaluated emperically. Consider a hypothesis that the relationship between p and y along AF is similar in various flow conditions except as scaled by the factors $(p_s - p_j)$ and $(1 - C_c)a$. That is, hypothesize that

$$\frac{p - p_j}{p_s - p_j} = F[n] \text{ where } n = \frac{y}{(1 - C_c)a}$$

or

$$\int_{F..A} p\,dy = -(1 - C_c)a\,(p_s - p_j) \int_0^1 F[n]\,dn - (1-C_c)a\,p_j$$
$$= -(1 - C_c)a\,\{(p_s - p_j)\,\Psi + p_j\} \qquad (23)$$

where Ψ is to be found experimentally.

Substituting the integrals from equations (21), (22) and (23), using Bernoullis equation (8) and the continuity relation equation (9), and simplifying leads to

$$C_c = \frac{1}{2} - \frac{1}{\pi}\left(F_b\,[b/a,\ v_1,\ v_2] - 2\,C_c\,\mathrm{Tan}^{-1}\,[v_a/v_j]\right) - \frac{1 - C_c}{2}\left(1 - \left(\frac{v_a}{v_j}\right)^2\right)\Psi \qquad (24)$$

where $F_b\,[b/a,\ v_1,\ v_2]$

$$= b/a\ \left(\left(\frac{v_1}{v_j}\right)^2 \mathrm{Tanh}^{-1}\,[v_1/v_a] + \mathrm{Tanh}^{-1}\,[(v_a v_1)/v_j^{\,2}] - \left(\frac{v_2}{v_j}\right)^2 \mathrm{Tanh}^{-1}\,[v_2/v_a] - \mathrm{Tanh}^{-1}\,[(v_a v_2)/v_j^{\,2}]\right) \qquad (25)$$

Equation (24) represents the one form of the development of the postulated theory with one approximation, the velocity at D.

<u>Adapting The Theory</u>

Equation (24) is not very useful in its present form. One difficulty is that this theory is for the 2-dimensional case whereas the tested model and real machines are 3-dimensional. This aspect primarily concerns the air gap which, counting the depth of air gap for each row of vent ducts, is much deeper than the vent duct in the direction normal to Figure 5.

McNown and Hsu (2) reported that experiments verified their predictions if the ratio b/a was given the value of the ratio of the areas of the channel and lateral duct respectively. This suggests that the increase in depth in the actual 3-dimensional channel is somehow equivalent to an increase in width, b, of the 2-dimensional mathematical theory. It is not known how much is an equivalent increase. However, this question does not need to be answered, since, if the term $F_b\,[b/a, v_1, v_2]$, is considered it can be shown (Appendix 3) that as b/a increases, $F_b\,[b/a, v_1, v_2]$ approaches a limit given by

$$\lim_{b/a \to \infty} F_b[b/a, v_1, v_2] = C_c \left(\frac{(v_1/v_j)^2}{\{1 - (\frac{v_1}{v_a})^2\}\,\frac{v_a}{v_j}} + 2\,\frac{v_1}{v_j}\,\mathrm{Tanh}^{-1}[v_1/v_a] + \frac{v_a/v_j}{1 - (\frac{v_a v_1}{v_j^2})^2} \right) \tag{26}$$

For typical values of the variables this limit approximates $F_b[b/a, v_1, v_2]$ with adequate accuracy before b/a reaches the ratio of areas of the air gap channel and duct.

Replacing the term in equation (24) with the limit from equation (26) and rearranging gives

$$C_c = \frac{1}{2} \left(\frac{1 - \psi\,(1 - (\frac{v_a}{v_j})^2)}{1 + F_c\,[v_1, v_a, v_j] - \frac{1}{2}\,(1 - (\frac{v_a}{v_j})^2)\,\psi} \right) \tag{27}$$

where

$$F_c [v_1, v_a, v_j] = \frac{1}{\pi} \{ \frac{(v_1/v_j)^2}{\{1 - (\frac{v_1}{v_a})^2\} \frac{v_a}{v_j}} + \frac{v_a/v_j}{1 - (\frac{v_1}{v_j})^2 (\frac{v_a}{v_j})^2} \tag{28}$$

$$+ 2 (\frac{v_1}{v_j} \mathrm{Tanh}^{-1} [v_1/v_j] - \mathrm{Tan}^{-1} [v_a/v_j])\}$$

Alternatively to equation (27)

$$\Psi = \frac{1 - 2 C_c (F_c [v_1, v_a, v_j] + 1}{(1 - C_c) (1 - (v_a/v_j)^2)} \tag{29}$$

from which Ψ can be computed from test data for v_1, v_a, v_j and C_c.

Data from quantitative tests when used in equation 29 revealed that, except near stalling conditions

$$.80 \leq \Psi \leq 1.1 \tag{30}$$

and that the velocity, v_a, varied little from a fixed ratio of v_j

$$.63 \leq v_a/v_j \leq .77 \tag{31}$$

The variation that did occur in these quantities was not correlated with other variables, and is readily explained as being due to experimental scatter.

Taking tentative values of Ψ and v_a/v_j at $\Psi = .95$ and $v_a/v_j = .70$ gives the equation

$$C_c = \frac{.258}{.758 + F_d [v_1/ v_j]} \tag{32}$$

where

$$F_d [v_1/v_j] = \frac{1}{\pi} \{ \frac{(v_1/v_j)^2}{\{1 - \frac{1}{.49} (\frac{v_1}{v_j})^2 \}.7} + \frac{.7}{1 - .49 (\frac{v_1}{v_j})^2} \tag{33}$$

$$+ 2 (\frac{v_1}{v_j} \mathrm{Tanh}^{-1} [v_1/(.7v_j)] - .6107) \}$$

Equation (32) is plotted on Figure 7 and it may now be tested with experimental data. However, it is not directly useable in designing because usually v_1, and v_d, the mean duct velocity, would be given and C_c and/or v_j would be required. The preferred form of the equation is therefore

$$\frac{v_j}{v_1} = F_1 [v_1, v_d]$$

$$C_c = F_2 [v_1, v_d]$$

$F_1 [v_1, v_d]$ and $F_2 [v_1, v_d]$ are not readily obtained from equation (32) as mathematical expressions. However they can be obtained graphically, because

$$\frac{v_d}{v_1} = \frac{C_c}{v_1/v_j} \qquad (34)$$

Therefore for every point on the curve in Figure 7 there exists a unique value of v_d/v_1, and C_c or v_j/v_1 may be plotted against that value to express $F_1 [v_1, v_d]$ and $F_2 [v_1, v_d]$. These functions are plotted in Figure 8 which provides convenient values for the contraction coefficient or jet velocity once the ratio of the air gap velocity to the mean duct velocity are known.

QUANTITATIVE TESTS

Preparation of the Model

Quantitative measurements assisted in the exploration and testing of the hypothesis formed. The duct on the side of the armature coil that was downstream with respect to the air gap was selected as a test duct. The flow patterns observed on both sides of the coil were similar, differing only slightly in degree, but the downstream duct was more representative because there were two ducts upstream of it while the other path saw only one duct upstream.

Two rows of holes through the view plate and close to the two walls of the duct provided taps for static pressure readings, (Figure 9). Also pressure taps were provided downstream of the armature coil and in the plenum beyond the duct. A pitot impact tube was used for each of the four paths, so that the proportion of air flowing in each path could be determined. A pressure tap was located adjacent to each impact tube and another in the air gap channel opposite to the armature coil.

The pressures were scanned by a motor-driven multiple-port valve (Scanivalve) which connected each in turn to a variable-reluctance transducer whose output was amplified and recorded. A micro-manometer connected to one of the pressure taps provided a calibration of the record. Figure 10 shows the model with the pressure measuring equipment.

A miniature hot-wire anemometer probe mounted on a micrometer was arranged such that it could traverse the duct at the location (shown in Figure 9) where the vena contracta had usually been observed. Because of external obstructions it crossed at about 10° from normal to the duct.

The probe was operated by a constant temperature anemometer bridge whose output was read by a digital integrating voltmeter using 1 second integrating periods. The probe had been previously calibrated in a calibrating nozzle with the same bridge and voltmeter.

All the instruments that were used are listed in Appendix 4.

Volume Flow Rate Measurement

The flow from the air gap was drawn through a test duct provided with a sharp-edged orifice. The flow from the ventilating duct, that is, the total flow from both sides of the armature coil, was drawn through a second test duct and orifice. The flow from the two guard ducts was drawn through a third orifice. Manometer readings of pressure drop across the orifices provided measures of the three air flows.

Test Method

Each test consisted of recording all the pressures, recording the flow rate pressures, and recording the anemometer voltage both D.C. and R.M.S. at various probe locations. The only serious problem in the tests was the fluctuation in pressure and velocity. Pressures fluctuated over a range of up to 4% in many tests and up to 10% in tests near the stalling conditions.

27 tests were made at a wide range of conditions:

v_1 from 45 to 140 ft/sec.

v_d from 0 to 80 ft/sec.

v_d/v_1 up to 1.5

A map of the test conditions is shown as Figure 11. The duct on the upstream side of the armature coil was blocked for three tests. The armature coil was moved to increase duct width from .4375 to .62 inches and the duct upstream of the armature coil was blocked for another three tests. The temperature in the vicinity of the model and the barometric pressure were recorded at least once on every test day.

Test Data Analysis

(1) Volumetric flow rates in the three test ducts were calculated in accordance with standard flow measurement methods[6] to obtain

Q_2	-	flow rate from air gap	ft^3/min
Q_d	-	flow rate from vent ducts	ft^3/min
Q_g	-	flow rate from the guard ducts	ft^3/min

(2) Impact heads were read to obtain h_{d1} and h_{d2} for the vent ducts downstream and upstream respectively of the armature coil and h_{g1} and h_{g2} for the guard ducts downstream and upstream respectively of the vent ducts.

(3) Flow rate in the tested vent duct was obtained from

$$Q_{d2} = Q_d \left(\frac{(h_{d2})^{1/2}}{(h_{d2})^{1/2} + (h_{d1})^{1/2}} \right) \quad ft^3/min \qquad (35)$$

and for the guard duct downstream of the vent duct

$$Q_{g2} = Q_g \left(\frac{(h_{g2})^{1/2}}{(h_{g2})^{1/2} + (h_{g1})^{1/2}} \right) \quad ft^3/min \qquad (36)$$

(4) Flow rate upstream of the tested duct was obtained from

$$Q_1 = Q_2 + Q_{d2} + Q_{g2} \qquad ft^3/min$$

Velocities were then obtained from the following equations

$$v_1 = \frac{Q_1}{A_g\,(60)} \qquad \text{ft/sec} \qquad (37)$$

$$v_d = \frac{Q_{d2}}{A_{d2}\,(60)} \qquad \text{ft/sec} \qquad (38)$$

A_g = cross-sectional area of air gap channel = .00972 ft^2

A_{d2} = cross-sectional area of one vent duct = .001135 ft^2 in all tests except the "wide duct" tests for which it was .001608 ft^2.

(5) Significant pressures were recorded or a profile of pressure along the duct was drawn.

The loss in the rounded entrance to the air gap channel and along the channel itself was negligible. This was readily demonstrated by a total head pitot tube which at the corner A produced zero reading with respect to atmosphere. Tests revealed that the static pressure in the air flowing at the corner was the same as the pressure just inside the eddy. Therefore

$$\rho \frac{v_a^{\,2}}{2} = p_o - p_s \qquad (39)$$

where p_o is the atmospheric static pressure

p_s is the pressure in the eddy

or

$$v_a = 66.75 \left(\frac{h_o - h_s}{r} \right)^{1/2} \qquad (40)$$

where $(h_o - h_s)$ is the change in static head from atmospheric to the eddy in inches of water and r is the ratio of density at the given state to density at N.T.P.

(6) A profile of velocity across the duct was drawn. Then the jet velocity v_j and contraction coefficient C_c could be determined from equations

$$Q_{d2} = \int_0^{C_c a} v \, dy \qquad (41)$$

$$v_j = \frac{v_{d2}}{C_c} \tag{42}$$

y being measured from the jet side of the duct. Usually v_j was obvious in an inspection of the velocity profile.

Velocity Profiles

Figure 12 shows a typical velocity profile. The velocities measured very close to the left wall, which were influenced by the hole from which the anemometer probe emerged, together with the apparent boundary layer on the left wall have been ignored.

A region of approximately uniform velocity representing the jet is seen to occupy one side of the profile. The turbulence in this region is relatively low - less than 10%. The width of the jet, defined by the coefficient of contraction, varies with flow conditions, and vanishes in the stalling condition.

The velocity decreases from the velocity of the jet in a mixing zone adjacent to the jet. The width of the mixing zone is a nearly uniform fraction of the duct width. As the velocity decreases the turbulence ratio increases to a peak of 35% to 45%.

A zone of approximately uniform velocity and decreasing turbulence extends from the mixing zone to the wall of the duct. The anemometer used did not distinguish direction of flow, but it is obvious that the flow in the jet contributes the majority of the flow through the duct while the other two zones form a large eddy. The air in low velocity zone must travel toward the inlet.

Pressure Profiles

Figure 13 shows two typical pressure profiles. One was obtained close to the wall above the jet, and the other was obtained close to the wall above the eddy.

On the eddy side the static pressure is uniform from the inlet to near the attachment point. It then rises continuously to a value, at the downstream end of the armature coil, that is close to the pressure at discharge from the duct.

On the jet side the pressure is relatively high at the inlet and then falls rapidly. At about the vena contracta the pressure profile has zero gradient and then it rises being indistinguishable thereafter from the profile on the eddy side. The low static pressure on the jet side that must accompany the high velocity jet was never observed in the pressure profiles. However, a small, square-cut tube inserted through the view plate about the mid-height of the duct at the vena contracta did sense a low static pressure at roughly the value one would expect.

DISCUSSION

Test Data

The values of significant velocities and pressures that were measured and of derived quanties such as v_j, C_c, v_a and Ψ are given in Table 2. For convenience some data are plotted.

In Figure 14 Ψ and v_a/v_j are plotted against C_c.

In Figure 15 γ, the ratio of the pressure drop in the vent duct to the velocity head in the jet is plotted against C_c.

In values of C_c are also plotted on Figures (7) and (8) which also shows the curves predicted by theory. It is seen that the agreement between test data and theoretical predictions for C_c and v_j/v_1 is reasonably good. This agreement applies also to the tests on single ducts and single wide ducts.

The agreement McNown and Hsu observed between free streamline theory and experiment is in contrast to the findings of this investigation. Perhaps in the experiments they report, in which water was the working fluid, a gas-filled pocket occurred instead of the quiescent zone. If so the free streamline theory would have been applicable.

TABLE 2

Test No.	3B	3C	5A flow stalled	4C	2B	3B repeat not used	4B leaky not used	5B	6B flow stalled
h_o	2.00	3.53	4.08	4.54		2.40	4.25	4.90	4.95
h_1	.46	1.63	.38	1.32	.47	.42	.53	.65	.3
h_s	-.67	-1.95	-.50	-1.95	-.49	-.72	-.68	-.93	-.5
h_d	-.05	-.21	-.02	-.17	-.042	-.01	-.049	+.012	-.1
v_1	75.7	88.4	129	117.2	45.2	80.2	126.2	134.9	140.9
v_d	31.3	66.8	0	66.6	37.4	34.8	27.5	23.0	0
v_j	156	210	145	252	120	153	195	210	140
C_c	.201	.318	0	.264	.311	.227	.141	.1095	0
v_a	103.8	153.9	128	169.6	79.4	105.2	145.3	158.9	153
Ψ	1.10	.98		.90	.89	.93	1.32	1.56	

TABLE 2 (cont'd)

Test No.	2A	2A	3A	2.9A	2.9.A.1	3.1.A.1	3.2.A.1	2C	2D
	not used	repeat							
h_o	.76		1.74	1.26	2.12	2.09	2.89	1.82	2.50
h_1	.18		.22	.18	.37	.34	.44	1.12	1.75
h_s	-.24		-.29	-.23	-.50	-.53	-.55	-1.16	-1.77
h_d	-.015		-.025	-.02	-.05	-.045	+.017	-.17	-.25
v_1	45.9	46.2	78.9	72.5	74.0	84.5	101.3	48	53.1
v_d	19.8	20.3	14.8	15.9	26.9	25.9	17.3	58.8	79.6
v_j	100	100	120	122	143	154	158	172.1	208
C_c	.198	.203	.123	.130	.188	.168	.1095	.341	.373
v_a	63.0		84.2	92.2	96.8	106.2	121	115.2	137.8
Ψ	1.06		1.34	1.42	1.11	.99	1.67	.97	.83

TABLE 2 (cont'd)

Test No.	3.9.C	3.1.C	3.BIDB	3.CIDB	3BWD	3CWD	4BWD	4AIDB
			One Duct		One Wide Duct			One Duct
h_o	4.67	3.05	2.20	3.63	2.16	2.96	4.15	4.68
h_1	1.22	1.25	.55	1.78	.46	1.16	.50	.23
h_s	-2.11	-1.59	-.59	-1.10	-.55	-1.10	-.66	0
h_d	-.32	-.22	-.08	-.05	-.21	-.28	-.42	0
v_1	114.8	89.0	82.3	86.9	83.6	89.6	123.5	141.5
v_d	65.5	63.8	36.6	62.1	26.7	46.3	29.8	15 approx.
v_j	268	226	162	202	155	181	211	No jet
C_c	.243	.282	.226	.308	.1725	.254	.141	None
v_a	173.2	143.5	111.2	145.0	109.9	134.2	146.1	-
ψ	.92	.85	.86	.86	1.05	.83	1.00	-

Notes for TABLE 2

(a) h_o, h_1, h_s, h_d = static heads-inches water - relative to discharge from duct

(b) v_1, v_d, v_j, v_a = velocities ft/sec.

The Mixing Zone

The analysis identified the existence of a mixing zone very similar to the free jet boundary that Schlichting (Reference 5, page 689) describes in a review of work by Goertler and Reichardt's work. Schlichting gives an equation for the velocity distribution across the mixing zone

$$v = \frac{v_o + v_i}{2} \{ 1 + \frac{v_o - v_i}{v_o + v_i} \operatorname{erf} [\xi] \} \tag{43}$$

$$\xi = \sigma y/s$$

where v_o and v_i are the velocities on each side of the mixing zone.

s is the distance to the origin of the zone

y is measured from the zone's midpoint.

σ is an empirical constant found by Riechardt to be 13.5.

In the vent duct the mixing zone was not straight and velocities v_o and v_i were not constant along the mixing zone. Nevertheless, if s is taken as the distance along the jet boundary to the origin of the zone at the corner of the armature coil and if v_o and v_i are taken as the jet velocity and zero respectively, then equation (43) accurately predicts the velocity distribution observed in the mixing zone.

The free jet boundary theory leads to the expectation that the mixing zone width will be constant at a given station for various flow conditions, and tests on the vent duct confirmed this.

The mixing zone phenomenon is probably primarily significant as a concept in fluid mechanics analysis. The foregoing analysis has shown how it can be used like free-stream theory to develop theories of "discontinuous" flows.

The Quiescent Zone

The region between the mixing zone and the wall farthest from the jet, tacitly assumed to be stagnant or quiescent, is actually a region of moderate velocity which often exceeded the mean duct velocity. It might be supposed that the velocity in this zone is determined by the flow in the mixing zone which in turn is determined by the jet velocity v_j. Therefore it can be written that

$$v_s \, (1 - C_c - C_m)a \;=\; v_j \, \chi C_m \, a \qquad (44)$$

where v_s is the velocity in the quiescent zone

$C_m a$ is the width of the mixing zone

χ is a factor to be evaluated.

With the mixing zone width measured from the boundary of the jet to the point of minimum velocity, test data indicated that

$$.268 \leq C_m \leq .365 \qquad (45)$$

and its average value was .323. Using a value of .323 for C_m and the value of C_c predicted in Figure 8, χ was computed for each test and was found to lie between .2 and .3 and vary randomly in that range. Thus v_s can be predicted approximately by

$$\frac{v_s}{v_j} = \frac{.323}{(.677 - C_c)} \, \chi \qquad (46)$$

$$.2 \leq \chi \leq .3$$

The "quiescent" zone will probably contribute significantly to transfer of heat from the armature coil and the iron near the duct inlet.

Stall

The velocity distributions observed across the duct showed that the mixing zone and quiescent zone persisted when flow in the duct stalled. The highest velocity in the mixing zone, at the wall in this case, was 1.0 to 1.12 times the average air gap velocity. The situation could be described by saying that the flow pattern of the other tests persisted except that the contraction coefficient became zero.

Apparently the eddy comprising the mixing zone and the quiescent zone, in the duct that was being observed, sustained a pressure difference, Δp, over the length of the duct that was sufficient to cause the required flow in the other duct.

If the ratio, γ defined by

$$\gamma = \frac{2\Delta p}{\rho v_j^2}$$

is considered, and plotted against C_c it is seen (in Figure 15) that γ decreases as C_c is reduced by reducing v_d/v_1. The relationship between γ and C_c is not known, except empirically, and cannot be found for $0 < C_c < .11$ because stalling precludes testing in that region. The pressure difference is the velocity head of the jet minus the regain of velocity head to static head in the turbulent region downstream of the vena contracta. This regain is apparently affected by C_c and possibly, when C_c is very small, the regain process becomes inefficient. One reason for this would be that the mixing zone, whose width remains constant at all flows, might tend to dominate the jet at small values of C_c, and to absorb the kinetic energy of the jet. Therefore, γ might increase as C_c is decreased below about .11, which is consistent with Figure 15. It would also explain why, when C_c reaches .11, the flow would not be shared equally between two (or more) ducts, but that one would stall and the remainder would carry all the flow.

To test this theory one test was made with only one duct open and the velocity ratio $v_d/v_1 \approx .106$ and surprisingly, no jet or eddy was formed in this case. The velocity was nearly uniform across the duct and the fluid was very turbulent.

It is apparent that if the pressure difference applied to a duct is small the state of flow is instable because:

(a) if no jet and eddy exist then flow will proceed into the duct obeying a relation like

$$p_a = \frac{1}{C_d^{\,2}} \rho \frac{v_d^{\,2}}{2} \tag{47}$$

where C_d is a coefficient of discharge

p_a is the pressure difference in this case.

C_d is likely to have a value of about .55 giving

$$p_a \approx 4. \frac{\rho}{2} v_d^{\,2} \tag{48}$$

but (b) if flow exists a jet and eddy will form requiring the pressure difference to be

$$p_b = \gamma \frac{\rho}{2} v_j^{\,2} \tag{49}$$

where p_b is the pressure in case b.

Test data, showed that near stall $\gamma \approx .06$, (Figure 15) and $v_d/v_j \approx .1$

so

$$p_b \approx 6. \frac{\rho}{2} v_d^2 \tag{50}$$

and therefore $p_b > p_a$.

Hence, if the applied pressure is between p_b and p_a, the flow is instable and might be expected to oscillate between these states producing the small net flow and the high turbulence that were observed. Consequently, γ cannot be measured for $0. < C_c < .11$.

All actual machines have many vent ducts in parallel and therefore as the average value of v_d/v_1 is lowered below .15 an increasing number of vent ducts may be expected to stall, and heat transfer would be greatly impaired in the vicinity of each stalled duct.

Relation to Heat Transfer Coefficients

The results of this investigation will be useful for studies of heat transfer and its variation with position and other parameters. For example, it is well known that heat generation is far from uniformly distributed in the armature coil, or in the teeth between coils, because of the so-called "stray-load losses". This means that simple overall average heat transfer analysis will provide inaccurate answers in computation of temperatures, and therefore, local coefficients are needed. But, clearly, the investigation shows that local fluid flow conditions vary widely and, therefore the surface heat transfer coefficients can be expected to vary widely too.

While this investigation thus indicates a necessity for local measurement of heat transfer it also assists such an endeavour by identifying zones in which fluid conditions are constant or vary in a regular way. This should allow simpler heat transfer experiments to be designed. Also, the knowledge of magnitude of the fluid flow variables might be used to assess the local heat transfer coefficients in some zones.

Relation to Duct Design

Inevitably a knowledge of the flow details in the duct will lead to improved duct design. For example, it is often observed that the use of turbulence promoters on the surface enhances heat transfer. The knowledge of the detail flow conditions will assist in judgments as to whether turbulence promoters will help and where they should be located.

As another example, it was noted that the jet separated from the wall just downstream of the vena contracta. Downstream from the separation the high jet kinetic energy dissipates in the form of free-stream turbulence. This free-stream turbulence contributes little towards heat transfer while accounting for most of the pressure difference along the duct. This has suggested modifications in duct design that might dramatically reduce the resistance to flow. Preliminary tests on such a modification, which is described in an invention disclosure to the Canadian Westinghouse Co., have been encouraging.

Finally, a knowledge of the flow configuration should assist in judging the relative merits of variations in duct depth, number of vent fingers and their location and similar details.

Future Developments

The test rig and model built for this investigation can now be used to assist in heat transfer measurement. The base on which the model was built can be used but it is suggested that in future experiments the "armature coil" can be eliminated. This will provide more working room, which will be essential for accurate tests, and will simplify testing. Now that there is a better understanding of the flow configurations the results of simpler tests can be used to make more generalized correlations. More tests are required to refine the modifications to the duct to reduce the pressure difference along the duct.

CONCLUSIONS

(1) In a stator vent duct, because of the effect of the peripheral flow in the air gap, ventilating air will travel through the duct via a high velocity jet on one side of the duct accompanied by an eddy on the other side. The eddy is comprized of a mixing zone and a region of uniform velocity. Free-streamline theories are grossly inaccurate in predicting the conditions quantitatively.

(2) A theory is postulated and developed to obtain a relationship, in equation (24), of the form

$$C_c = F\,[b/a,\, v_a,\, v_1,\, v_2,\, v_j,\, \Psi]$$

Where Ψ is an empirical factor.

(3) Tests show that Ψ and the ratio v_a/v_j are constant or nearly so. Using mean values and making an approximation which adapts the 2-dimensional theory to 3-dimensional circumstances produces a simplified relation, in equation (32), of the form

$$C_c = F\,[v_1,\, v_j]$$

(4) By plotting in Figure 8 relationships are found in the form

$$C_c = F\,[\, v_d/v_1 \,] \qquad\qquad v_j/v_1 = F\,[\, v_d/v_1 \,]$$

which relationships will be useful in design of machinery or design of heat transfer experiments.

(5) The width and velocity distribution in the mixing zone is close to that predicted by Schlichting (5) in his review of Goertler's and Riechard's work.

(6) The velocity, v_s, in the uniform velocity zone in the eddy is approximately given, by equation (46), in the form

$$v_s/v_j = F [C_c, \chi]$$

where χ is an empirical term found to lie between .2 and .3.

(7) The flow in a duct will stall when the ratio of duct velocity to air gap velocity, v_d/v_1, is reduced to the apparently critical value of .15.

(8) The results of the investigation are seen to have relevance both to heat transfer experiments and to ventilating duct design.

(9) The test rig and the model should be retained and used to measure heat transfer coefficients and to refine the invented duct modifications.

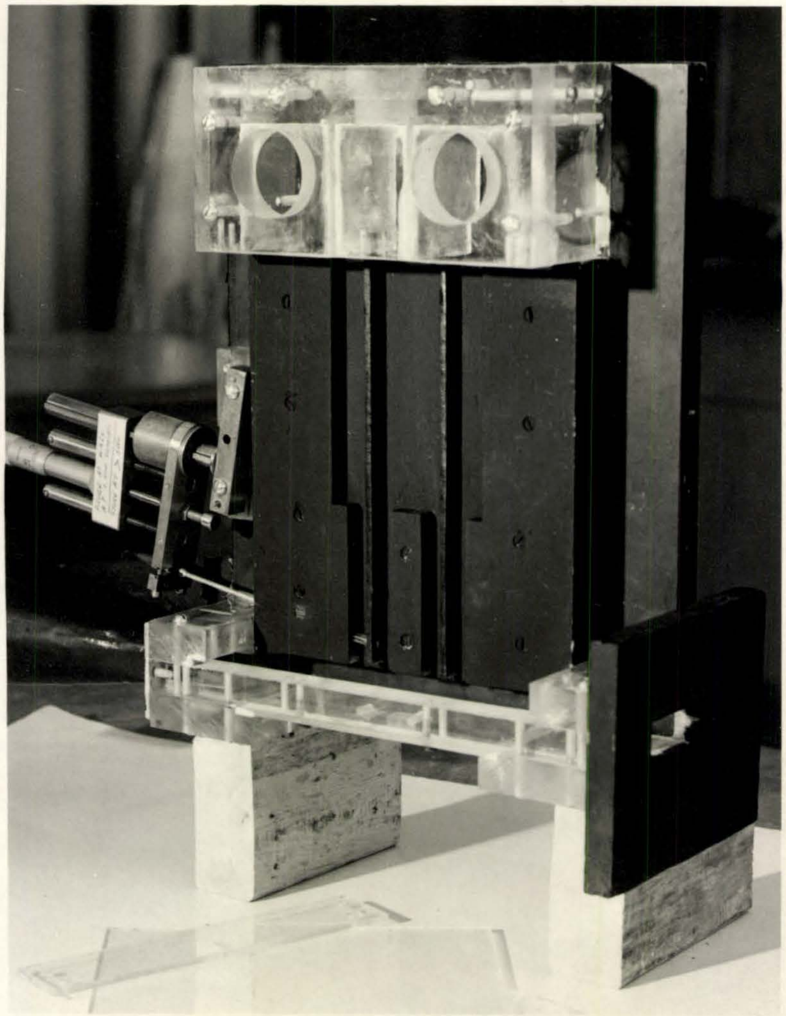

Ventilating Duct Model

Figure 1

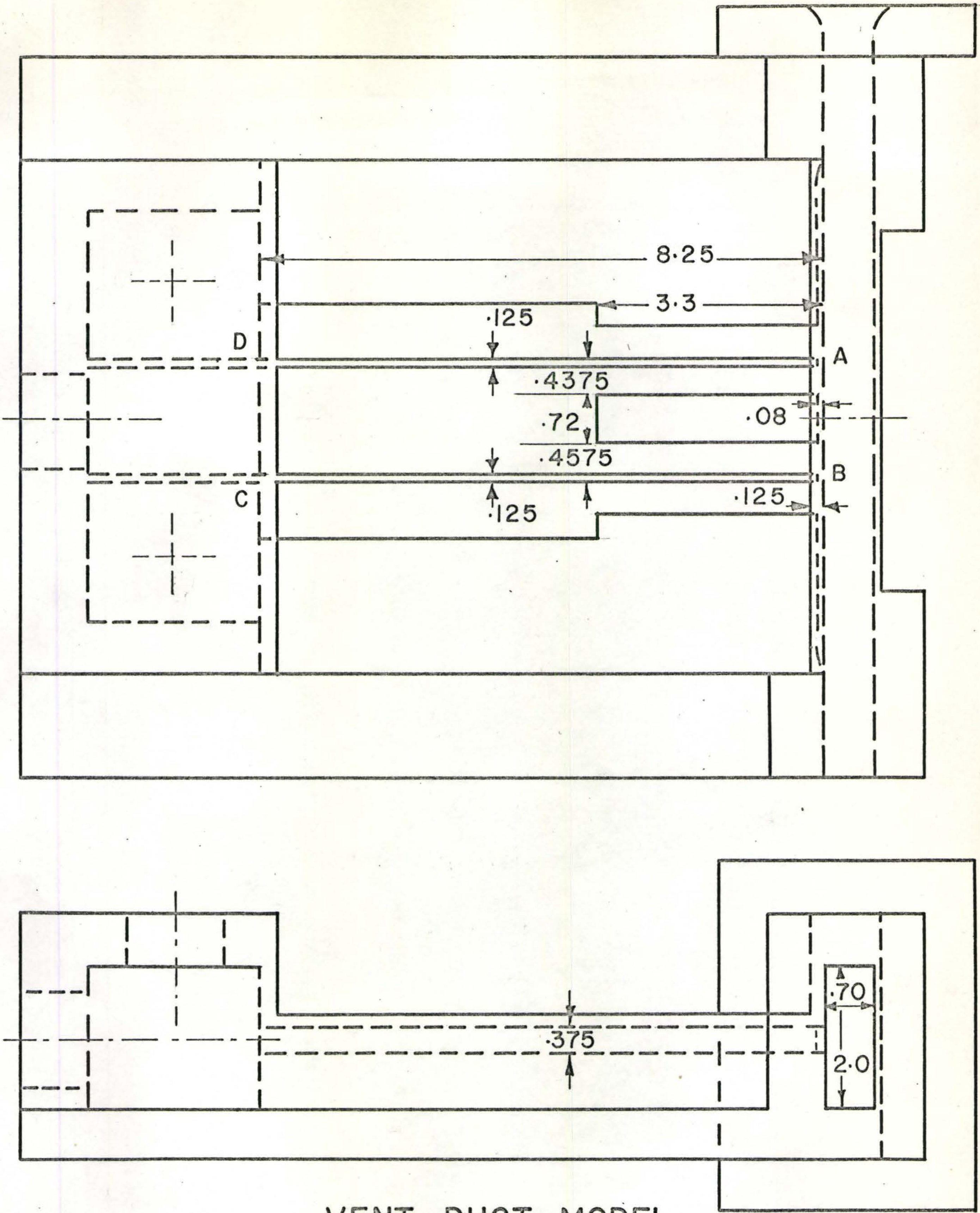

VENT DUCT MODEL
PRIMARY DIMENSIONS
(dimensions in inches)

FIGURE 2

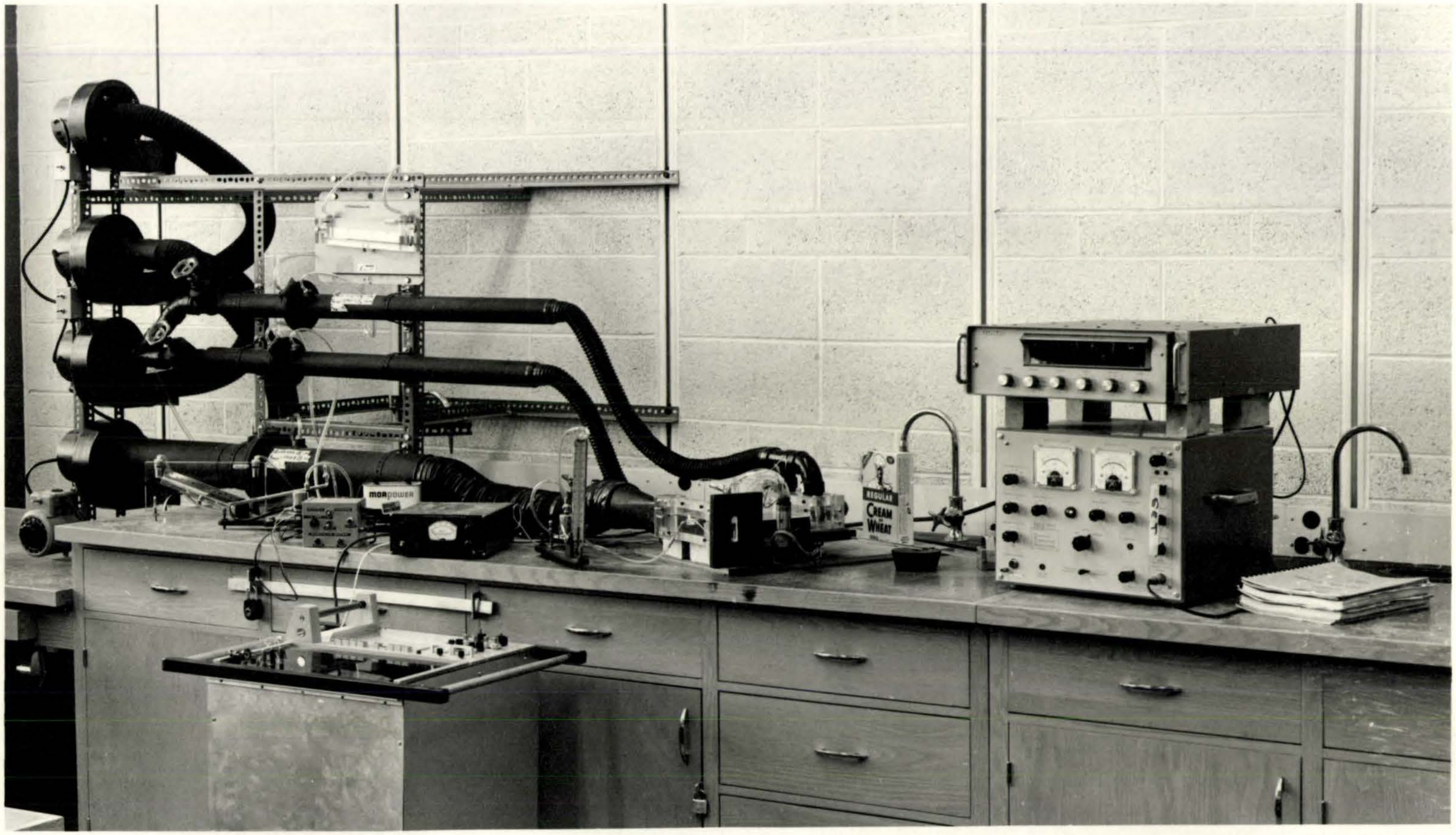

Test Rig, Model, and Instruments

Figure 3

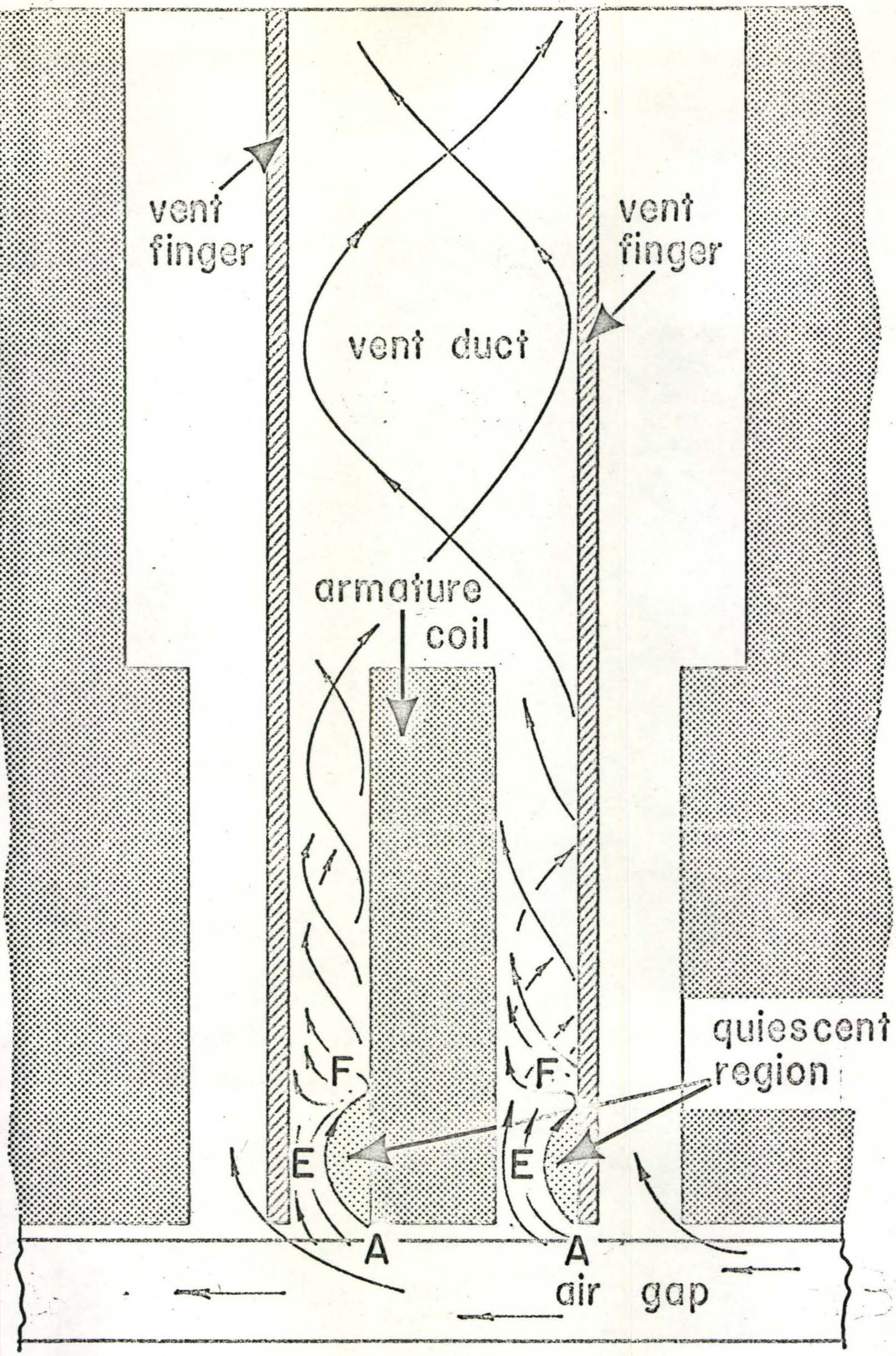

FLOW PATTERN IN VENTILATING DUCT

FIGURE 4

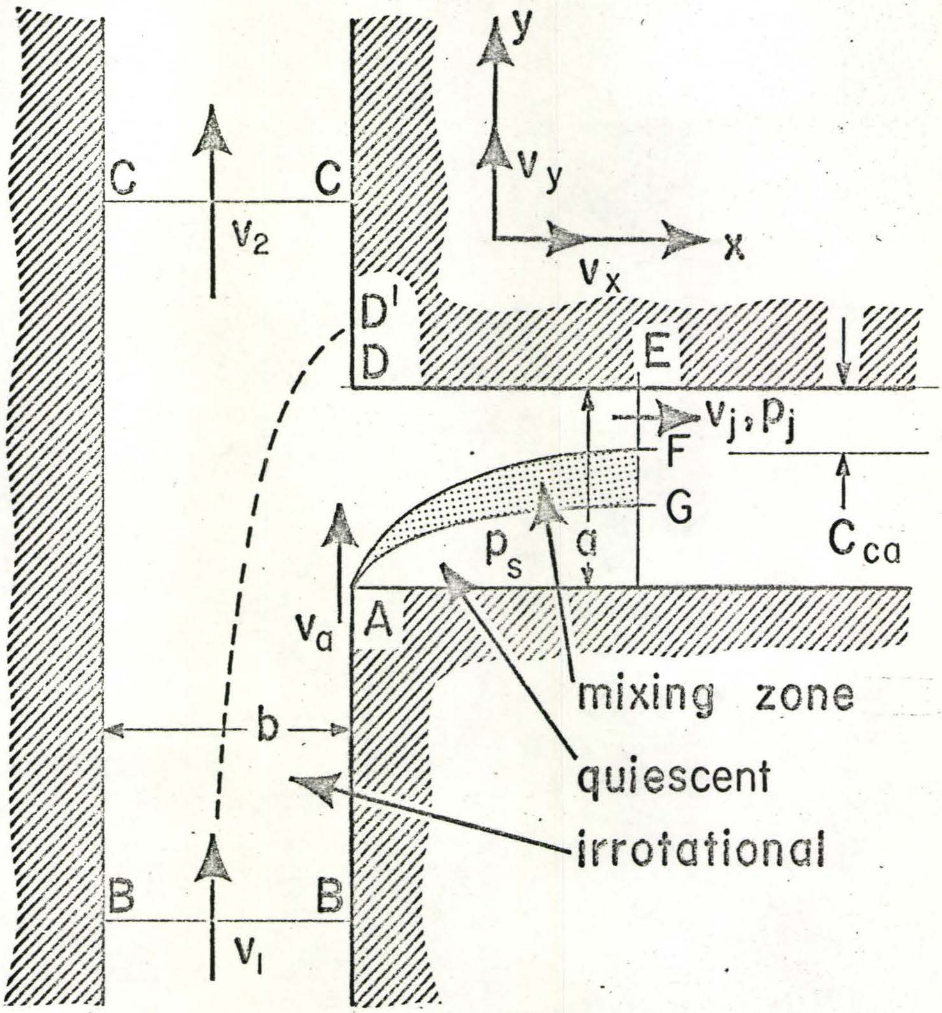

DIAGRAM OF POSTULATED FLOW

FIGURE 5

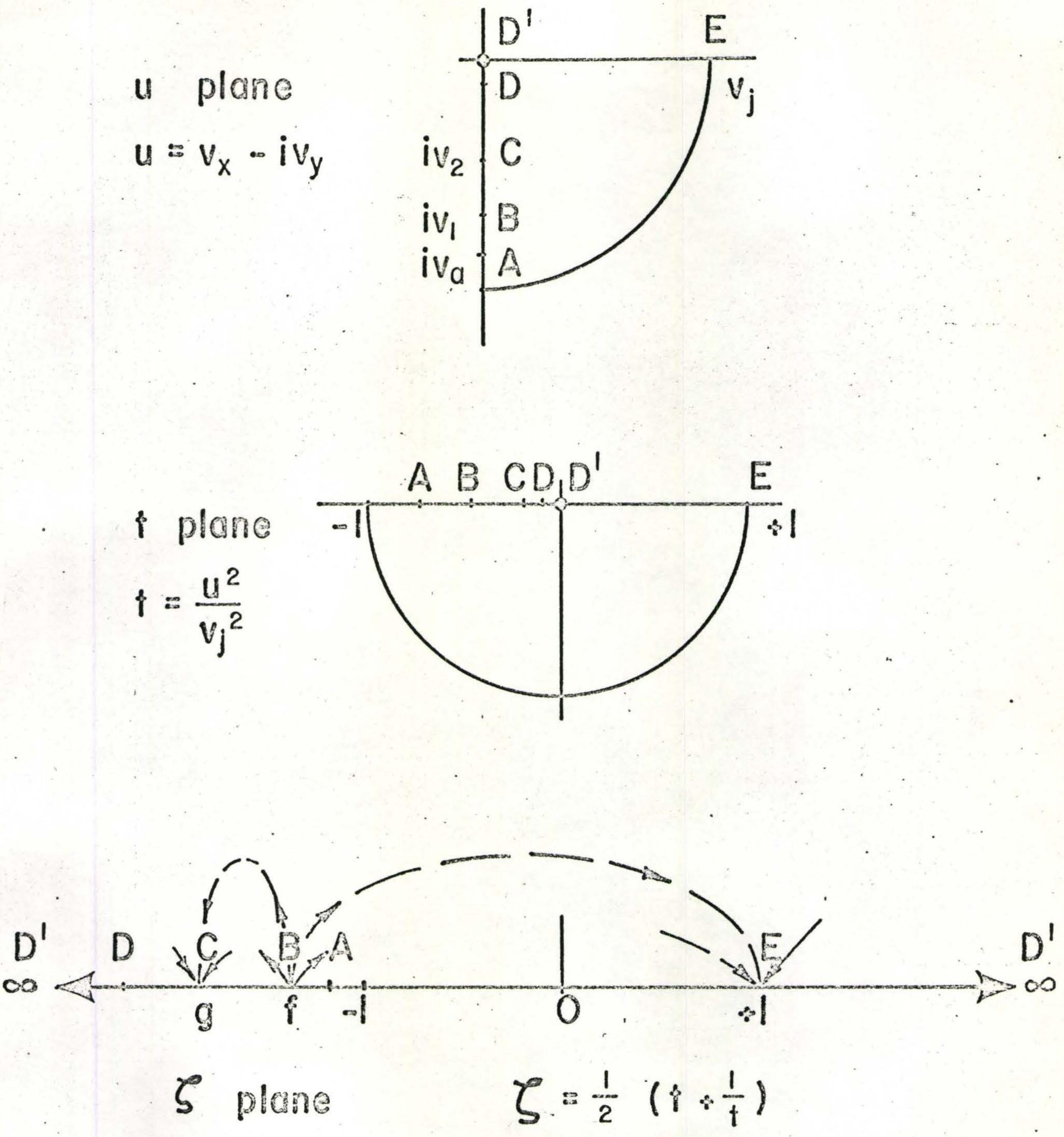

GRAPHIC DEPICTION OF THE CONFORMAL TRANSFORMATIONS

FIGURE 6

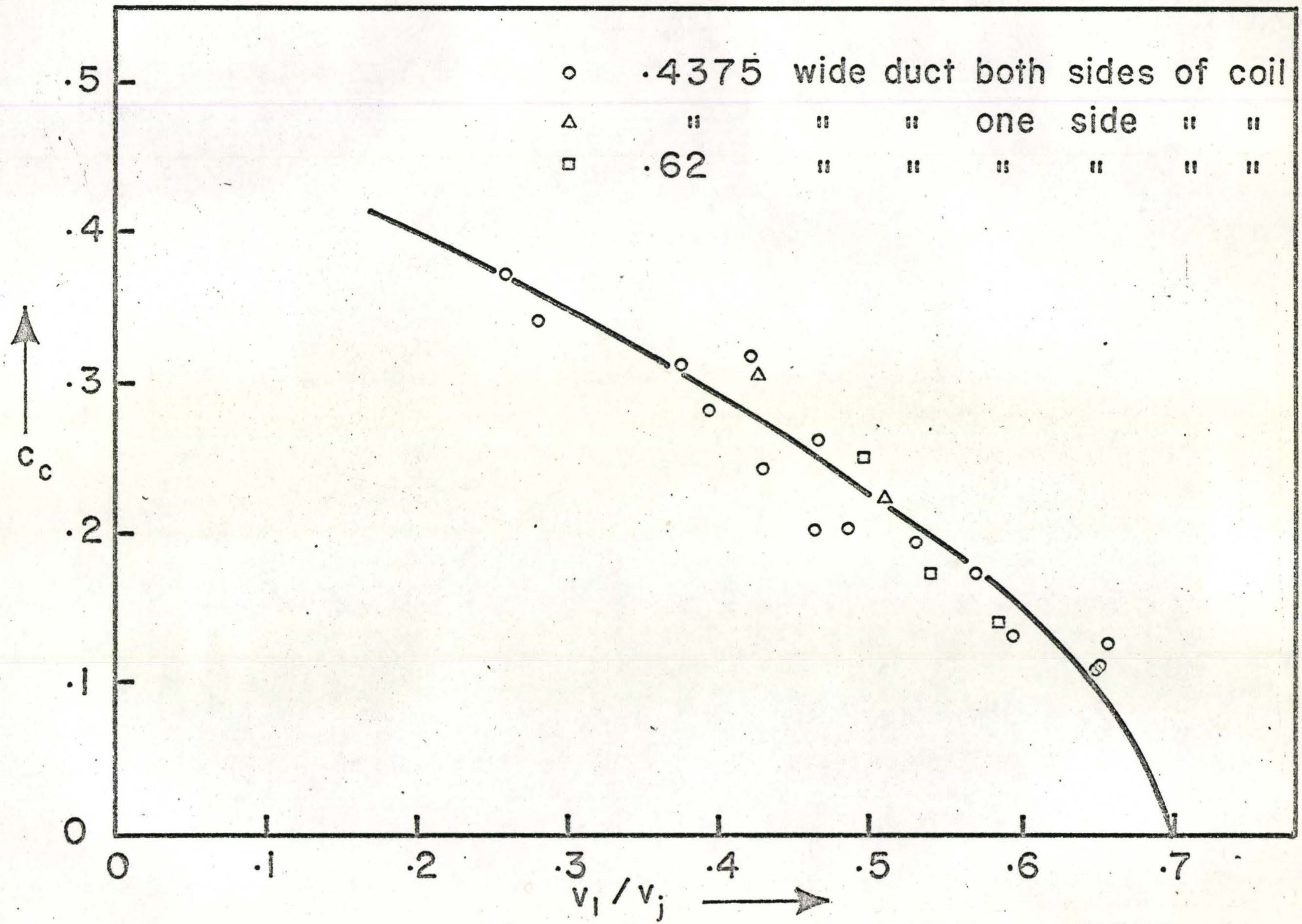

Relationship between contraction coefficient, c_c, and ratio of gap velocity to jet velocity, v_1 / v_j. Theoretical curve and test values are shown.

FIGURE 7

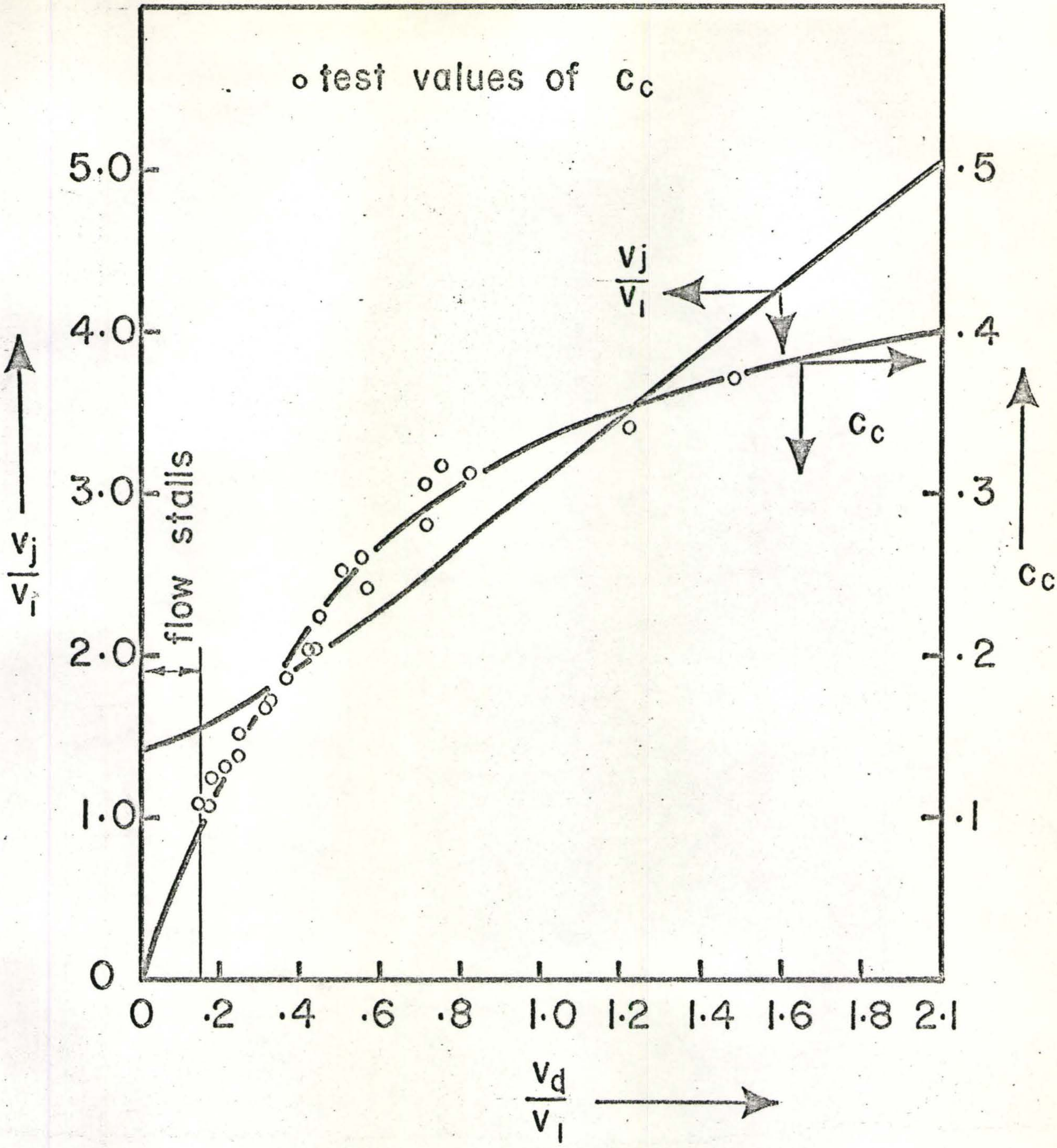

Ratio of jet velocity to air gap velocity, v_j / v_1, and contraction coefficient, c_c, for various ratios of mean duct velocity to air gap velocity, v_d / v_1. Theoretical curves and test values for c_c are shown.

FIGURE 8

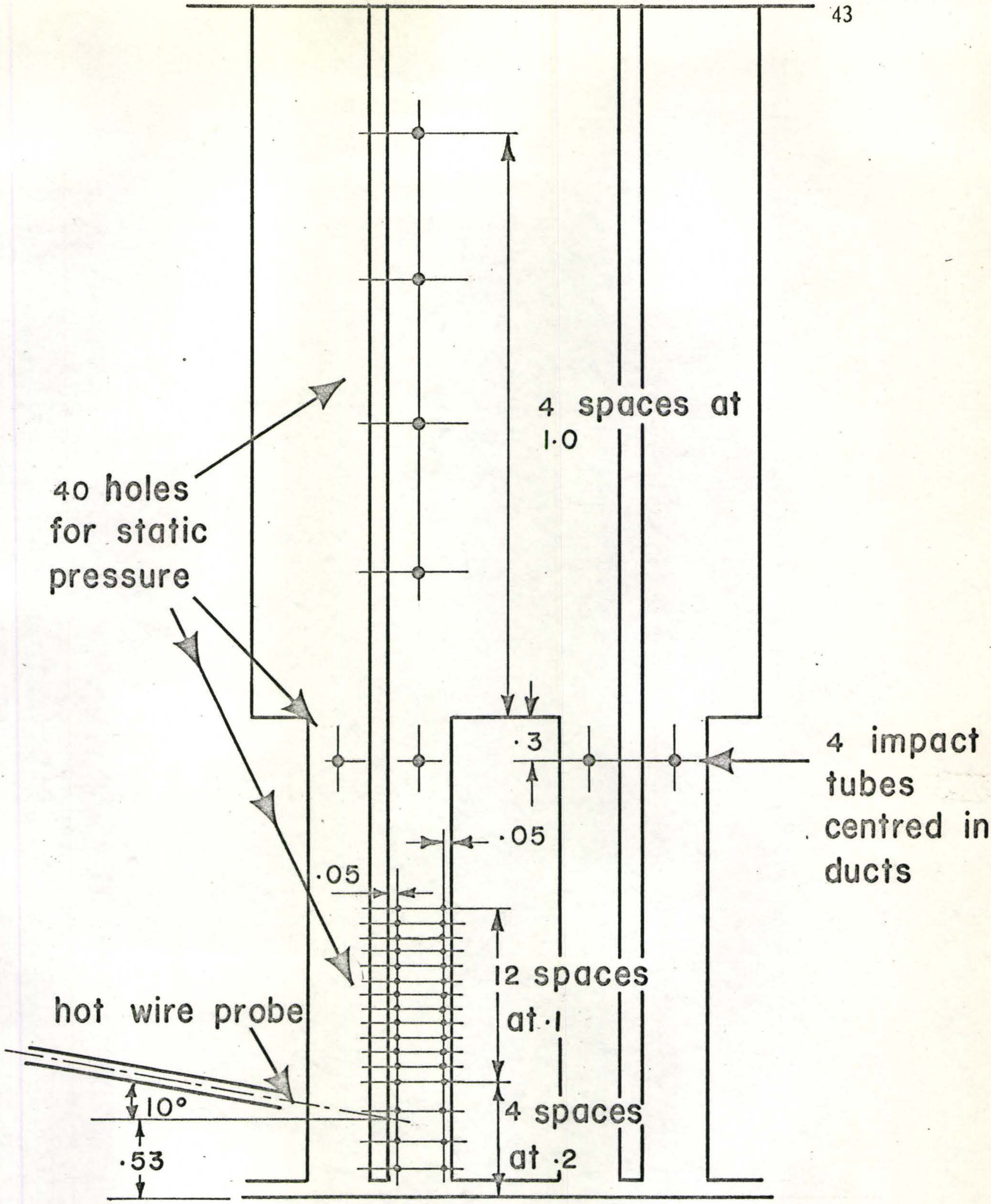

LOCATION OF INSTRUMENT
FACILITIES ON. VENT DUCT MODEL
(dimensions in inches)

FIGURE 9

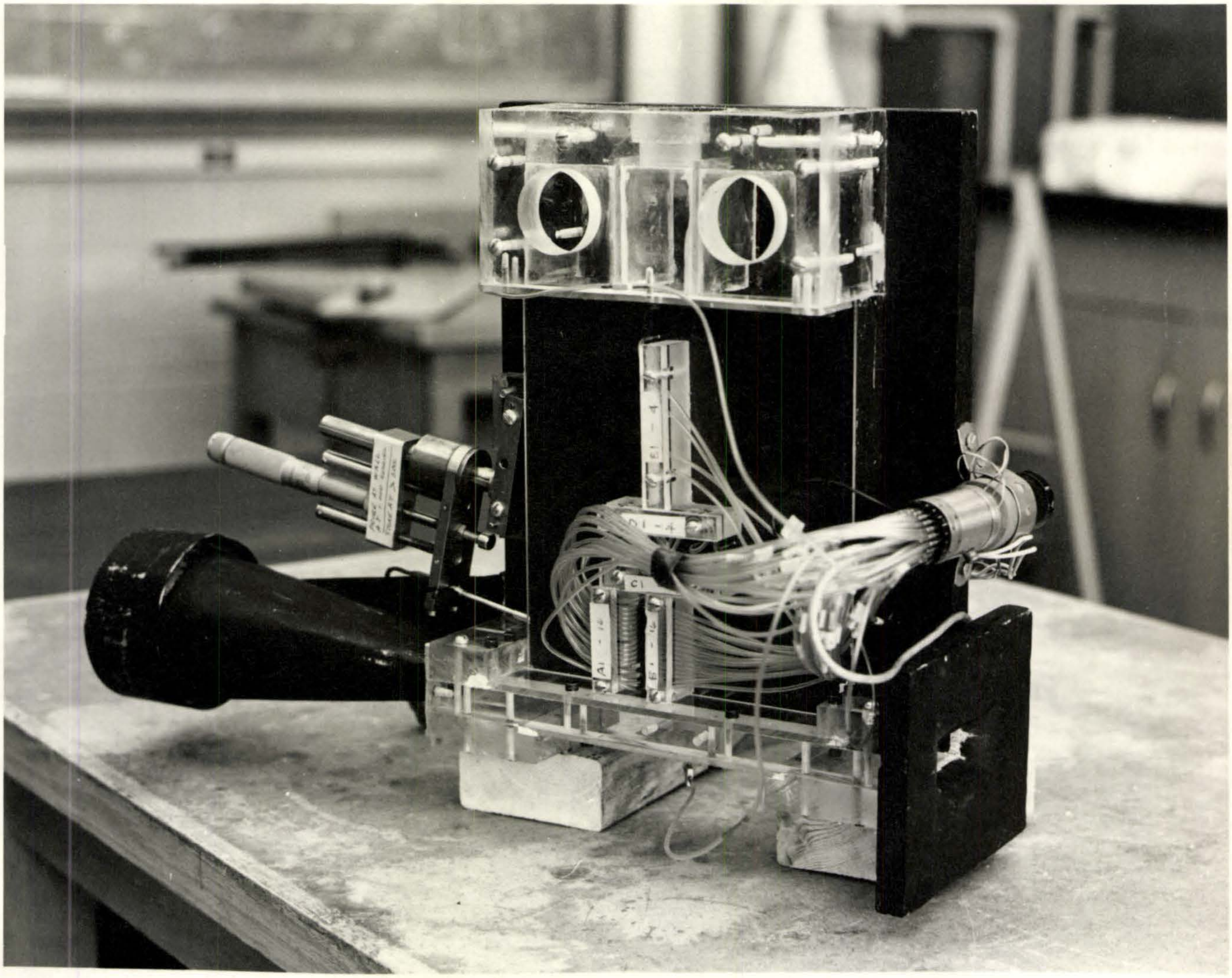

Model with Instrument Facilities

Figure 10

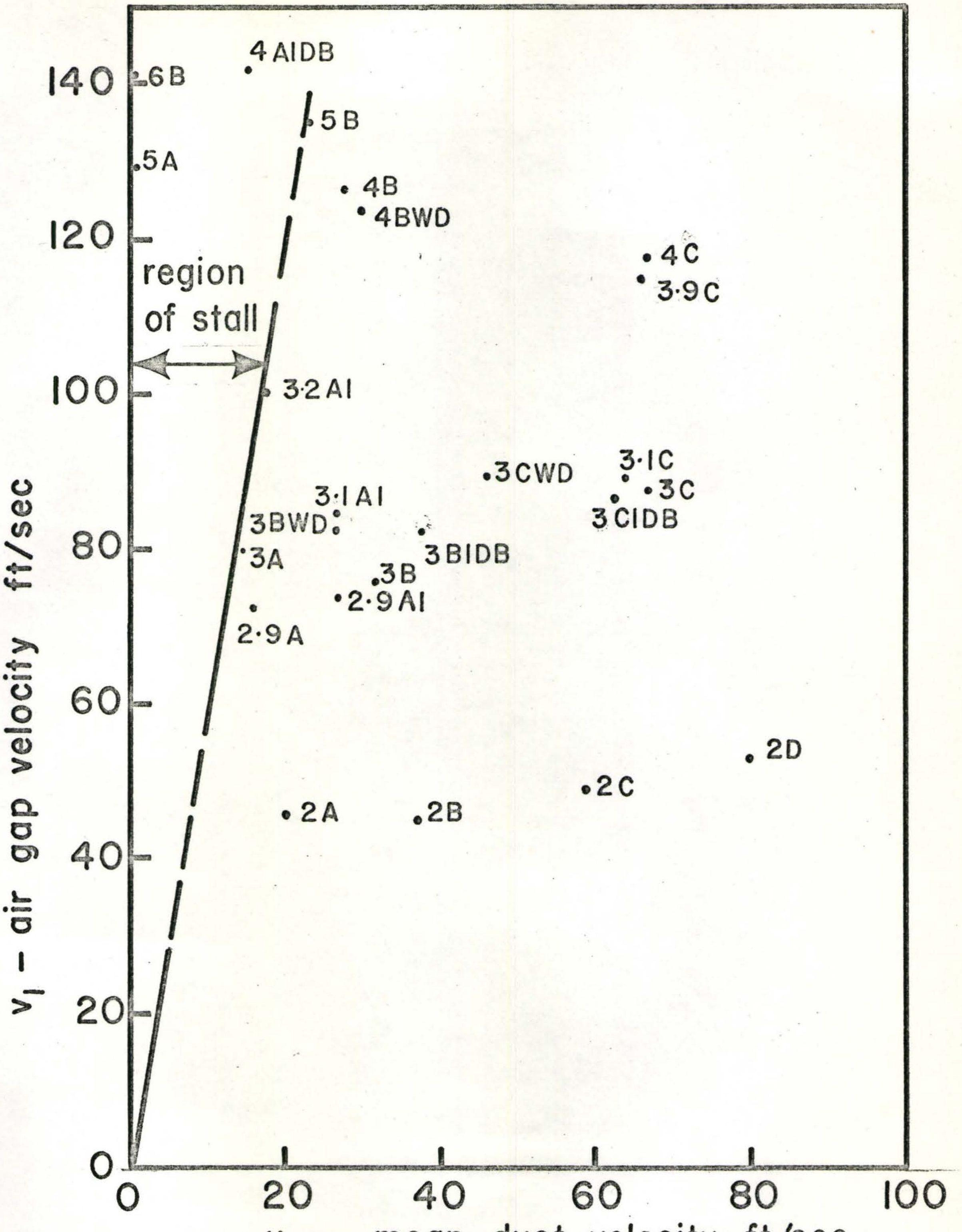

MAP OF TEST CONDITIONS

FIGURE II

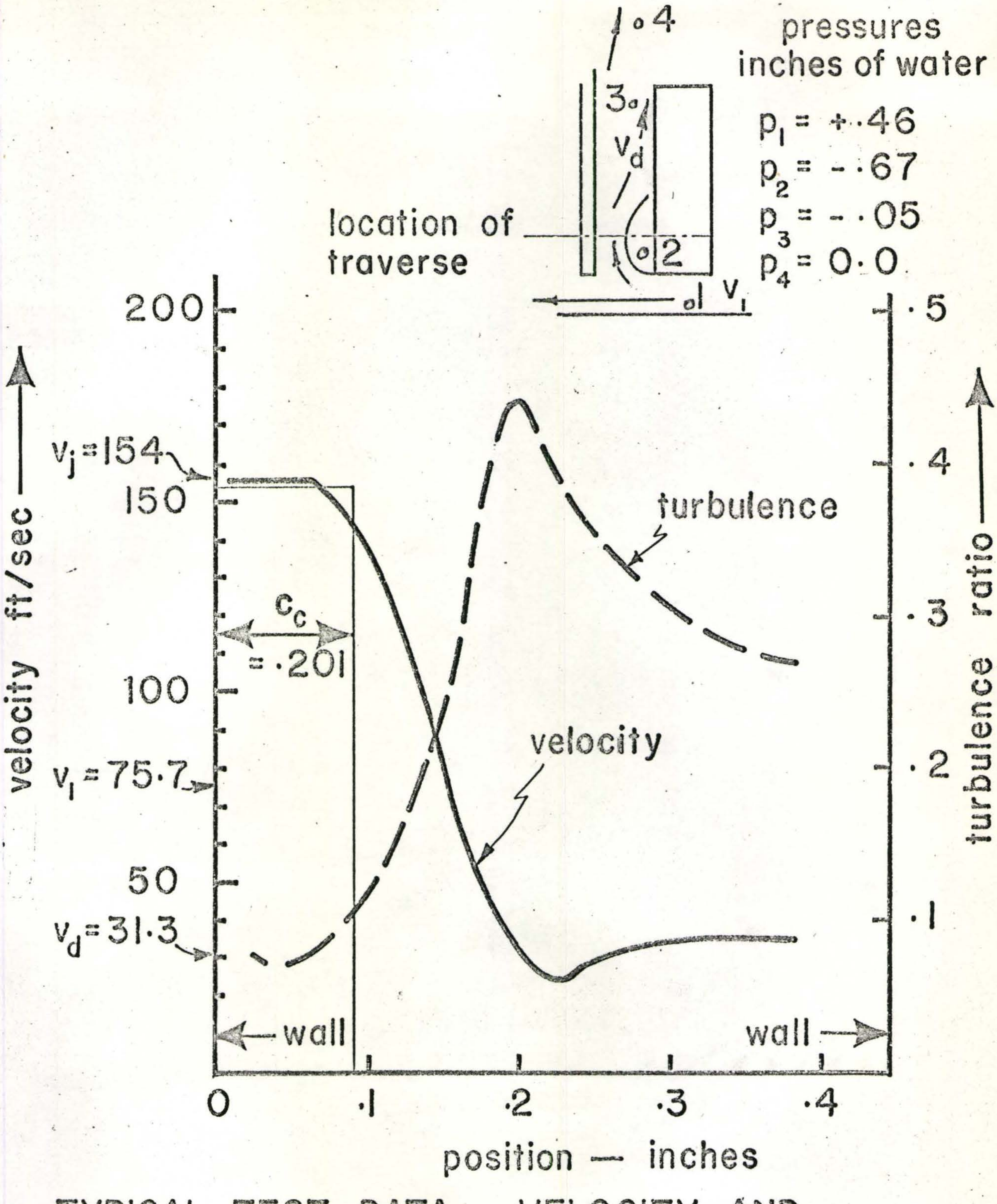

TYPICAL TEST DATA — VELOCITY AND TURBULENCE DISTRIBUTION AND PRESSURES

FIGURE 12

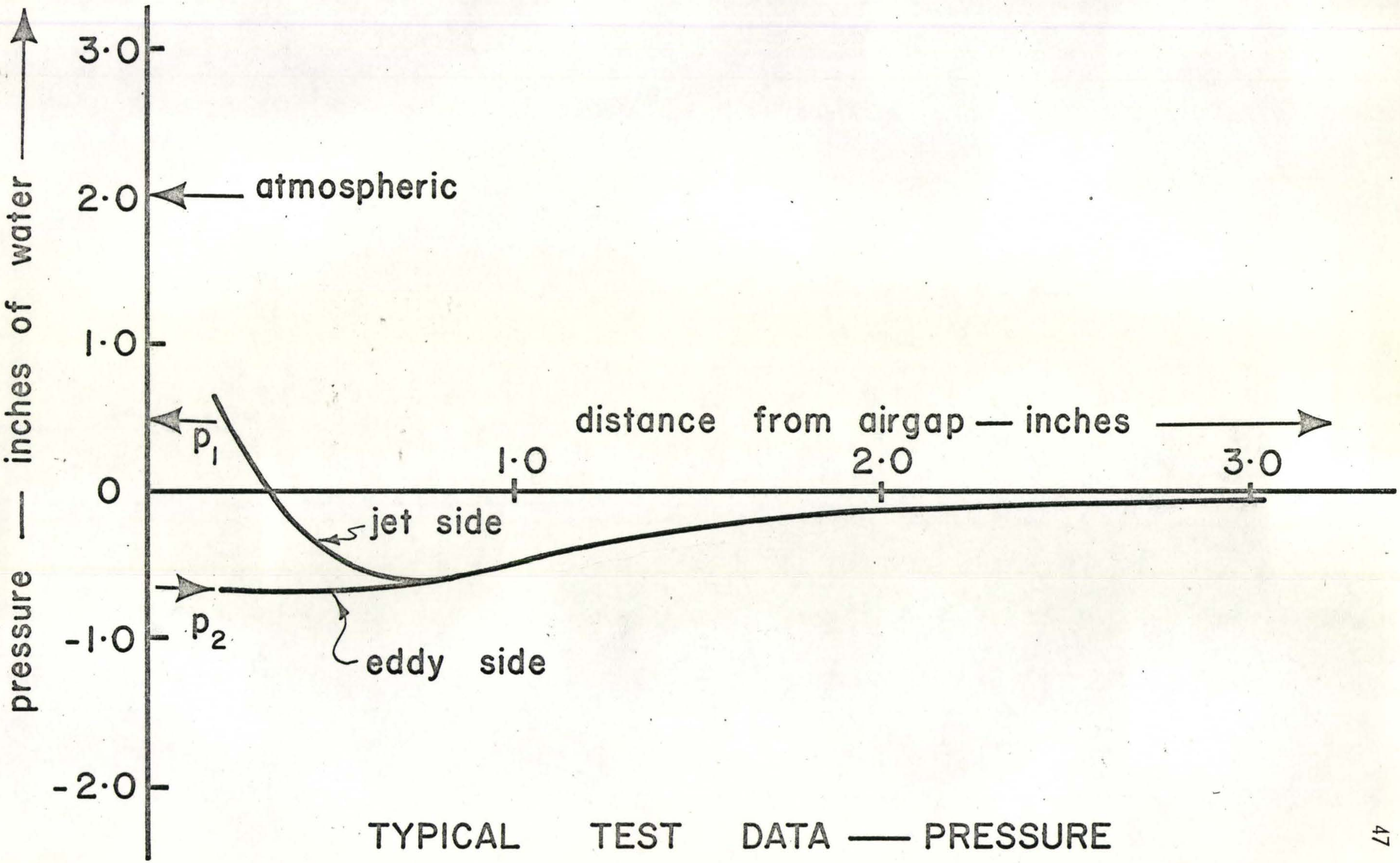

TYPICAL TEST DATA — PRESSURE DISTRIBUTION ALONG DUCT

FIGURE 13

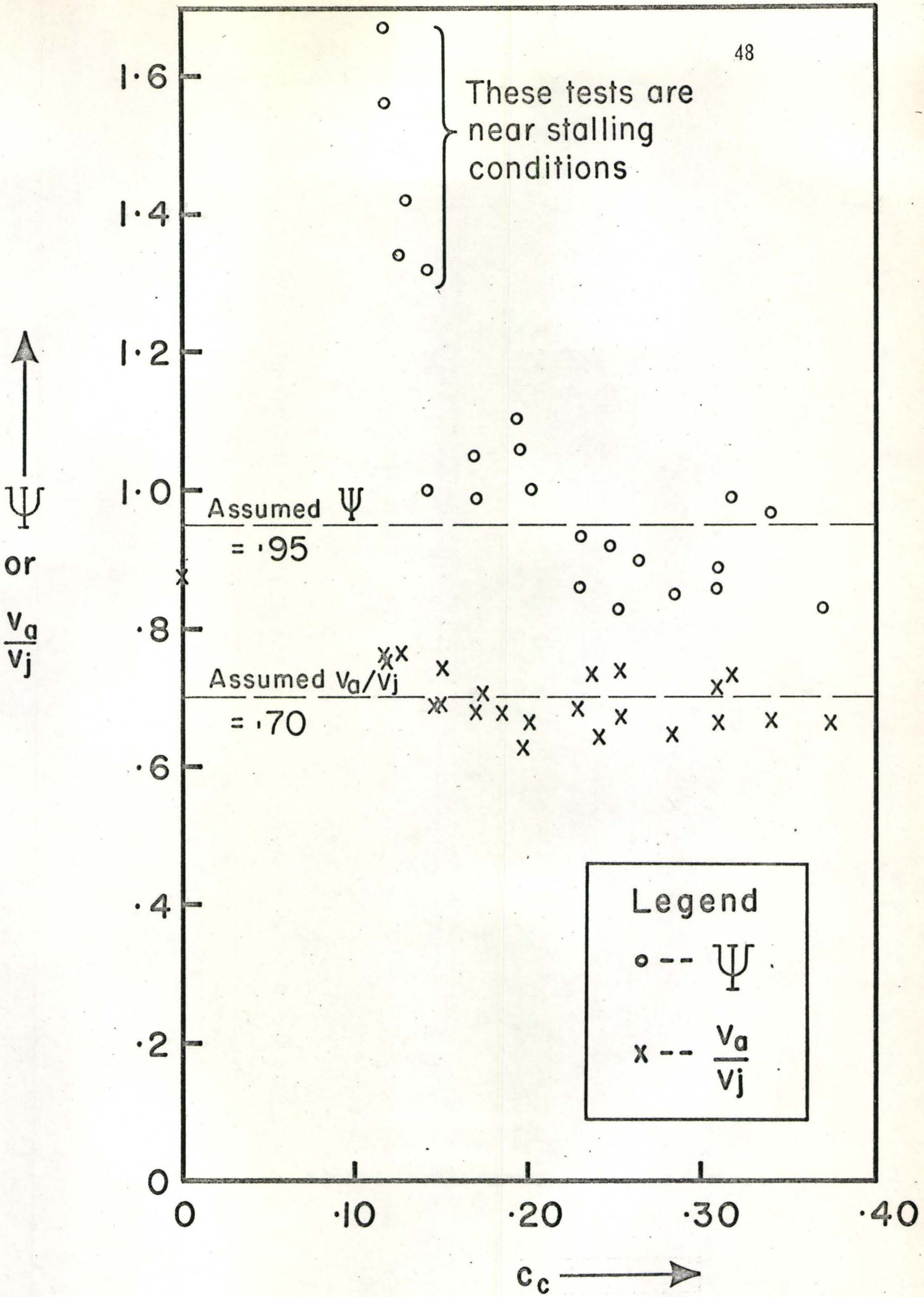

Test values of Ψ and the ratio v_a / v_j

FIGURE 14

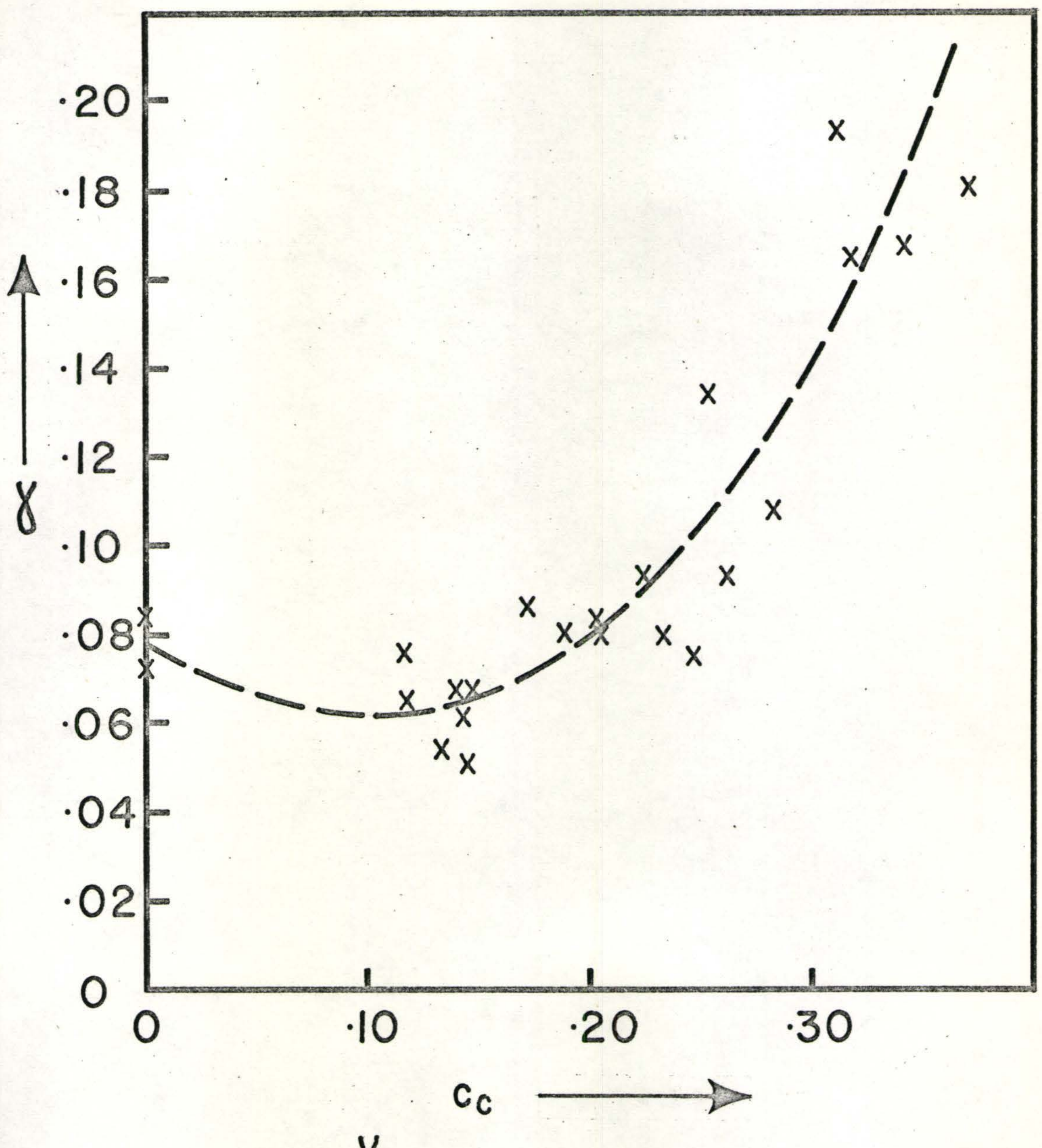

Values of γ found in various tests show a correlation with c_c

FIGURE 15

APPENDIX 1

Reduction of the integral

$$I_e[u] = \int_{-iv_a}^{0} \frac{\left(\frac{u}{v_j}\right)^4 - 1}{\left(\frac{u}{v_j}\right)^4 - 2e\left(\frac{u}{v_j}\right)^2 + 1} \, du$$

$$\text{where} \quad e = -\frac{1}{2}\left\{\left(\frac{v}{v_j}\right)^2 + \left(\frac{v_j}{v}\right)^2\right\}$$

This can be written as

$$I_e[u] = v_j \int_{-iv_a/v_j}^{0} \frac{\xi^4 - 1}{\xi^4 + b\xi^2 + 1} \, d\xi$$

$$\text{where} \quad \xi = \frac{u}{v_j} \qquad d\xi = \frac{du}{v_j}$$

$$\text{and} \quad b = -2e = \left(\frac{v}{v_j}\right)^2 + \left(\frac{v_j}{v}\right)^2$$

whence

$$(b - 2)^{1/2} = \left\{\left(\frac{v}{v_j}\right)^2 - 2 + \left(\frac{v_j}{v}\right)^2\right\}^{1/2}$$

$$= \frac{v}{v_j} - \frac{v_j}{v}$$

and

$$(b + 2)^{1/2} = \left\{\left(\frac{v}{v_j}\right)^2 + 2 + \left(\frac{v_j}{v}\right)^2\right\}^{1/2}.$$

$$= \frac{v}{v_j} + \frac{v_j}{v}$$

The integration can be solved using standard techniques giving, after simplification, the expression

$$I_e[u] = v_j \left[\xi + \frac{1}{2}\left(\frac{v}{v_j} - \frac{v_j}{v}\right) \mathrm{Tan}^{-1} \left[\frac{\left(\frac{v}{v_j} - \frac{v_j}{v}\right)\xi}{1 + \xi^2} \right] - \frac{1}{2}\left(\frac{v}{v_j} + \frac{v_j}{v}\right) \mathrm{Tan}^{-1} \left[\frac{\left(\frac{v}{v_j} + \frac{v_j}{v}\right)\xi}{1 - \xi^2} \right] \right]_{-iv_a/v_j}^{0}$$

$$= v_j \left\{ 0 - \frac{iv_a}{v_j} - \frac{1}{2}\left(\frac{v}{v_j} - \frac{v_j}{v}\right) \mathrm{Tan}^{-1} \left[\frac{\left(\frac{v}{v_j} - \frac{v_j}{v}\right)\left(-i\frac{v_a}{v_j}\right)}{1 - \left(\frac{v_a}{v_j}\right)^2} \right] \right.$$

$$\left. + \frac{1}{2}\left(\frac{v}{v_j} + \frac{v_j}{v}\right) \mathrm{Tan}^{-1} \left[\frac{\left(\frac{v}{v_j} + \frac{v_j}{v}\right)\left(-i\frac{v_a}{v_j}\right)}{1 + \left(\frac{v_a}{v_j}\right)^2} \right] \right\}$$

$$= -iv_j \left(\frac{v_a}{v_j} + \frac{v}{v_j} \mathrm{Tanh}^{-1} \left[\frac{v}{v_a}\right] - \frac{v_j}{v} \mathrm{Tanh}^{-1} \left[\frac{v_a v}{v_j^2}\right] \right)$$

APPENDIX 2

Reduction of the integral

$$I_e[u] = \int_{-iv_a}^{0} \frac{\left(\frac{u}{v_j}\right)^4 - 1}{\left(\frac{u}{v_j}\right)^4 - 2e\left(\frac{u}{v_j}\right)^2 + 1} du$$

where $e = 1$

The integral can be written in the form

$$I_1[u] = v_j \int_{-iv_a/v_j}^{0} \frac{\zeta^4 - 1}{\zeta^4 + b\zeta^2 + 1} d\zeta$$

where $\zeta = \frac{u}{v_j}$, $\quad d\zeta = \frac{du}{v_j}$

and $\quad b = -2$

whence $(b - 2)^{1/2} = (-4)^{1/2} = 2i$

and $\quad (b + 2)^{1/2} = 0$

which can be solved using standard techniques to give

$$I_1[u] = v_j \left[\zeta + \frac{2i}{2} \operatorname{Tan}^{-1} \left[\frac{2i\,\zeta}{1 + \zeta^2} \right] \right]_{-iv_a/v_j}^{0}$$

$$= v_j \left(0 - i\frac{v_a}{v_j} - i \operatorname{Tan}^{-1} \left[\frac{+2\frac{v_a}{v_j}}{1 - \left(\frac{v_a}{v_j}\right)^2} \right] \right)$$

$$= -iv_j \left(\frac{v_a}{v_j} + 2 \operatorname{Tan}^{-1} \left[\frac{v_a}{v_j} \right] \right)$$

APPENDIX 3

To obtain a simplified expression for

$$\lim_{b/a \to \infty} F[b/a,\ v_1,\ v_2]$$

Given a function F[q]

$$= \frac{1}{q} \left(\phi_1^2 \, \mathrm{Tanh}^{-1} \left[\frac{\phi_1}{\phi_a}\right] + \mathrm{Tanh}^{-1} [\phi_a \, \phi_1] - \phi_2^2 \, \mathrm{Tanh}^{-1} \left[\frac{\phi_2}{\phi_a}\right] - \mathrm{Tanh}^{-1} [\phi_a \, \phi_2] \right)$$

where

$$\phi_2 = \phi_1 - C_c q$$

and, in the nomenclature of the main paper

$$q = \frac{a}{b}$$

$$\phi = \frac{v}{v_j} \qquad \phi_2 = \frac{v_2}{v_j}$$

$$\phi_a = \frac{v_a}{v_j}$$

To find $\lim_{g \to 0} F[q]$

which is of the form $\frac{0}{0}$, we can write

$$F[g] = \frac{f[g]}{g[q]}$$

whence $\lim [\, F[q] \,] = \lim \left[\frac{f'[q]}{g'[q]} \right]$ L'Hopital's Rule

$$= \lim_{q \to 0} \left[\left(\frac{1}{1} \right) \left(-\phi_2^2 \frac{1}{1 - [\frac{\phi_2}{\phi_a}]^2} \left(\frac{-C_c}{\phi_a} \right) - \mathrm{Tanh}^{-1} [\frac{\phi_2}{\phi_a}] \, 2\phi_2 \, (-C_c) \right.\right.$$

$$\left.\left. - \frac{\phi_a}{1 - [\phi_a \phi_2]^2} (-C_c) \right) \right]$$

$$= C_c \left(\frac{\phi_1^2/\phi_a}{1 - (\frac{\phi_1}{\phi_a})^2} + 2\phi_1 \, \mathrm{Tanh}^{-1} [\frac{\phi_1}{\phi_a}] + \frac{\phi_a}{1 - (\phi_a \phi_1)^2} \right)$$

APPENDIX 4

INSTRUMENT LIST

1. 2 - test ducts - 2.2 in dia with .920 in dia orifice and D and D/2 taps.

   Computed flow rate $Q = 11.511 \ (h_w/r)^{1/2}$ cfm

   h_w = head inches of water

   r = ratio of density to density at N.T.P.

   - used for: - vent duct, guard ducts flow rates.

2. Test duct - 4.03 in. dia with 2.000 in dia orifice and D and D/2 taps.

   Computed flow rate $Q = 55.502 \ (h_w/r)^{1/2}$ cfm

   - used for - air gap flow rate

3. 4 - 3550 rpm fan-motor units with 5 in dia x 1 1/2 wide f.c. rotor Torrington Part No. A16474 with General Electric 1/6 H.P., 208 volt 1.04 amp 1 phase motor.

4. Dwyer 0 - 1.0 in inclined manometer

   - used for guard flow-rate measurement.

5. Dwyer 0 - 3.0 in inclined manometer

   - used for air gap flow-rate measurement.

6. 2 - E. Vernon Hill Type "C" Micro manometers (Note: S. G. of fluid specified .7970, actual fluid used had S. G. of .815 to .816.)

7. Scanivalve Model 48 D3 S/N 453 multiple port motor - operated valve. (control box manufactured ad-hoc).

8. Scanco PDCR $\pm$ .2 psi SN 437 variable reluctance pressure transducer.

9. Scanco No POCA3 - p-ducer oscillator-carrier-amplifier.

10. Hewlett-Packard Model 7702A Recorder with Model 8802A medium gain DC preamplifier.

Items 7, 8, 9, 10 used for recording pressures.

11. DISA Model 55A25 Miniature Hot-Wire Probe and
DISA Model 55A21 Probe Support.

12. DISA Model 55A01 Constant Temperature Anemometer.

13. Honeywell 6305 Digital Multimeter (used as integrating voltmeter).
Items 11, 12, 13 used to measure velocity.

14. DISA Model 55A60 Calibrating Unit used to calibrate items 11, 12, 13.

15. Nabisco Cream of Wheat "Regular" Farina used for particle path visual tests.

16. Meriam Model 34FB2 Micromanometer used to calibrate item 6.

REFERENCES

1. J. S. McNown, 1953, Transactions American Society of Civil Engineers, Paper No. 2714, Mechanics of Manifold Flow.

2. J. S. McNown and En-Yun Hsu, 1951, Proceedings of the First Midwestern Conference on Fluid Dynamics, Page 143, Paper No. 6, Application of Conformal Mapping to Divided Flow.

3. A. Toch and R. W. Moorman, 1953, State University of Iowa, Studies in Engineering, Page 63, Bulletin 35, Manifold Efflux.

4. J. M. Robertson, 1965, Hydrodynamics in Theory and Application, Prentice-Hall/Englewood Cliffs, N. J.

5. H. Schlichting, 1968, Boundary Layer Theory, 6th Edition, Translated by J. Kestin, McGraw-Hill, U. S. A.

6. British Standards Institute, B.S. 1042 - "Flow Measurement".